Communications Research Centre

MOVING RANDOM SURFACES AND CORRELATION ANALYSIS

by

M.J. Burke

ernment of Canada
artment of Communications

Gouvernement du Canada
Ministère des Communications

CRC REPORT NO. 1384

OTTAWA, MAY 1985

Canada

COMMUNICATIONS RESEARCH CENTRE

DEPARTMENT OF COMMUNICATIONS
CANADA

MOVING RANDOM SURFACES AND CORRELATION ANALYSIS

by

M.J. Burke
(Radar and Communications Technology Branch)

CRC REPORT NO. 1384

May 1985
OTTAWA

TABLE OF CONTENTS

MOVING RANDOM SURFACES AND CORRELATION ANALYSIS

by

M.J. BURKE

ABSTRACT

Five models of moving random surfaces with known velocity and known correlation function are described. The random surfaces are formed from an infinite set of plane waves with decorrelation arising from random temporal and spatial changes. It is shown that, if there are random spatial changes in the direction of motion, then speeds derived by the full correlation method of Briggs et.al.(1950) will be less than the true speed of the surface. Random spatial changes at right angles to the direction of motion are necessary if the axial ratio of the correlation ellipse is to be finite. From modeling of a multi-antenna array, it is shown that the correlation ellipse is the average of the various shapes within the surface as argued by Burke(1975). If temporal-series based on the various models are subjected to a high-pass filter before correlation analysis, the correlation speeds increase in value.

Temporal correlation functions from three of the models fail the requirements for full correlation analysis because the half-widths of the cross-correlation functions are, in general, greater than the half-widths of the auto-correlation function. However, from a survey of experimental ionospheric drift measurements, it is argued that radio interference patterns appear to have the form of one of these three models, viz., Model 2. For this model, correlation speeds increase with increasing antenna spacing and the correlation ellipse tends to line up with that antenna pair with the greatest spacing(Golley and Rossiter,1970), the straight line of the straight-line method of Briggs et.al., will not be straight(Sales and Bowhill,1962) and, as stated above, the speeds will be low(Wright and Fedor,1967;Sprenger and Schminder,1969).

It is shown that the similar-fades method(Variant 2 of Sprenger and Schminder,1969) gives a better estimate of the surface speed than does the correlation method.

1. INTRODUCTION

In this report five different models are developed for two-dimensional moving random surfaces with known velocity and known correlation function. Although this work was developed specifically to investigate the methods of ionospheric drift analysis, the models themselves are completely general and can be used wherever the case of a moving random surface arises.

Briggs and Page(1951) developed a method for forming pairs of random series with known correlation function, but their method cannot be extended to two-dimensional space nor do the time-series have a known velocity. Longuet-Higgins(1957a, b), from a consideration of random surfaces, has developed relationships for the statistical properties of these surfaces in terms of their correlation functions. The work in this report, in effect, complements his work in producing random surfaces with known correlation functions.

With respect to ionospheric drifts, radio waves diffracted or reflected from the ionosphere form an interference pattern at the ground. If the amplitude of this pattern is recorded as a function of time at 3 or more non-collinear points it is found that the time-series *fades* or varies with time. In addition, it is noted that, in general, a series is displaced in time relative to another. This time displacement or delay is assumed due to the movement or *drift* of the interference pattern over the ground. It is assumed that this movement arises from the movement of the ionosphere causing the diffraction or reflection of the radio waves. Ionospheric drift analysis is concerned with the measuring of the velocity of the interference pattern over the ground and, via the point source effect , the movement of the ionosphere producing the pattern. The point source effect postulates that the the ground pattern will move with twice the velocity of the ionosphere.

One well known method of ionospheric drift analysis is that of Briggs.et.al.(1950), referred to as full correlation analysis(FCA). This method of analysis is based on the auto- and cross-correlation functions of the time series and is described in detail in the next section.

The method of FCA is based on the assumption that the ionosphere behaves as a random diffracting screen, as proposed by Booker et.al.(1950). For this model it is assumed that the reflecting region of the ionosphere is more or less flat and, at or near this reflecting region, there exists a random screen of irregularities which impose random phase and/or amplitude changes on radio waves passing through the screen. This results in a random amplitude pattern being formed at the ground. A more detailed discussion of this work is given by Ratcliffe(1955) who also showed that, provided the screen is not too thick, the correlation function over the ground pattern is of the same form as that over the random screen.

Somewhat allied with the proposals of Booker et.al., Wright and Pitteway(1978) developed a method for generating random radio patterns by assuming a number of scatterers to be located in the ionosphere. Radio waves are reflected from these scatterers and their interference pattern at the ground determined. Motion of this pattern is achieved by moving the scatterers randomly but with a mean motion. However, as yet, the correlation function of this ground pattern as a function of the scatterers has not been derived nor is there any evidence that the real ionosphere behaves as proposed in their model.

While it is highly desirable that a mechanism be determined between the behaviour of the irradiated ionosphere and the observed ground pattern, it is considered that such work could delay the publication

of this report, perhaps indefinitely, and hence, is not considered here.

Another method for deriving the velocity of the ground pattern is that of similar fades analysis(SFA). This method is an intuitive method and has no theoretical support. However, it has been used by some workers in the field, e.g. Burke and Jenkinson (1957) and Sprenger and Schminder(1969), and the ionospheric velocities obtained have been found to be in good agreement with other (non-drift) methods. There are two variants of this method and it is the second approach that is recommended.The method originated in the 1950's because, without the availability of computers, it was a much simpler method than FCA. SFA is discussed in Section 3.

The random surfaces developed in this report are assumed derived from an infinite set of plane waves. Decorrelation is introduced by varying the frequency and wave-number of these waves or their amplitudes. The way in which decorrelation is introduced for each model is described in Section 4.

The analytic solution for the correlation functions and the properties of each of the five models are presented in Sections 5 to 9, respectively. Because the analytic solutions for some of the models are rather intractable, the properties of these particular models are derived from the modeling of time-series. The effect of filtering the time-series before FCA is included in the properties because of some disagreement over this feature with respect to ionospheric drift analysis. Sprenger and Schminder(1969) reported that high-pass filtering before FCA resulted in higher values of drift speed and that these values were in better agreement with speeds derived from meteor trails. On the other hand, Chandra and Briggs(1978) argued that the increase in speed after filtering was to be expected and did not imply that the speed was too low before filtering. Plots of contours of constant amplitude over a 41×41 antenna array are presented for each model for isotropic conditions. Correlation ellipses for these contours are also included. This work was included because Burke(1975) argued that the correlation ellipse represented the average of all the various shapes in the amplitude pattern. This proposal was contrary to the generally accepted belief that all the shapes in the pattern were approximately similar to that of the correlation ellipse. In reply, Briggs(1976), while agreeing with Burke's conclusion concerning amplitude patterns formed by the interference of a few radio waves specularly reflected from the ionosphere, disagreed with the conclusion if the pattern was random, e.g. as might be formed from the Booker et. al. model. In fact, it was this disagreement that prompted the need for the work presented here.

A summary of the properties of each model is given in Section 10 and, in Section 11, these properties are compared with those found from experimental data.

It will be shown in this report that, except for a particular case , velocities derived by FCA will be less than the true velocity of the random surface. On the other hand, SFA(Variant 2) is shown to give better estimates of the velocity. It should be noted that there is no dispute over the direction of motion derived by either of these methods, only the magnitude of the velocity derived by FCA.

It will also be shown that the conclusions about the effects of filtering before FCA depend on the parameters of the random pattern and that the significance of the correlation ellipse is more in keeping with Burke's proposal.

2. FULL CORRELATION ANALYSIS

The full correlation analysis of Briggs et.al.(1950) is based on the fact that, at least close to the maximum, the correlation function has the form of the function(in 1 direction)

$$F(Ar^2 - 2Hr\tau + B\tau^2), \tag{2.1}$$

where r is the spatial separation between the two observing points and τ is the time delay or lag. Because, in practice, it has been found that the correlation functions approximate to a Gaussian form and because the Gaussian form permits analytic solutions, this form will be used throughout this report. In this form the correlation function is

$$\rho_{r,\tau} = e^{-\frac{Ar^2 - 2Hr\tau + \tau^2}{2\sigma^2}}, \tag{2.2}$$

where σ is the half-width of the correlation function for 0.6065 the maximum value of correlation(ρ_m).

Briggs et.al. assumed that, if two spatial-series were taken a time τ' apart, the velocity of the pattern, V_d is

$$V_d = r_m/\tau', \tag{2.3}$$

where r_m is the displacement for maximum spatial cross-correlation.

From 2.2, the condition for maximum spatial correlation can be derived from the partial derivative with respect to r, for a delay τ'. Thus, for the first stationary condition

$$r_m = H\tau'/A$$

and

$$V_d = H/A. \tag{2.4}$$

Because, in practice, only temporal-series are available, Briggs et. al. showed how A and H could be derived from the temporal correlation functions, as shown by typical auto- and cross-correlograms in Figure 2.1. From the partial derivative of the cross-correlation function(2.2) with respect to τ, for a separation r', it can be shown that the maximum value of cross-correlation occurs for $\tau = \tau_m$, where

$$\tau_m = r'H. \tag{2.5}$$

From this relationship Briggs et.al. defined a velocity called the *apparent velocity*(V_a), where

$$\begin{aligned} V_a &= r'/\tau_m \\ &= 1/H. \end{aligned} \tag{2.6}$$

The word apparent arose because at first sight this velocity appeared to be the true velocity of the pattern but, as argued by Briggs et.al., if there are temporal changes within the pattern, then this velocity will be too high.

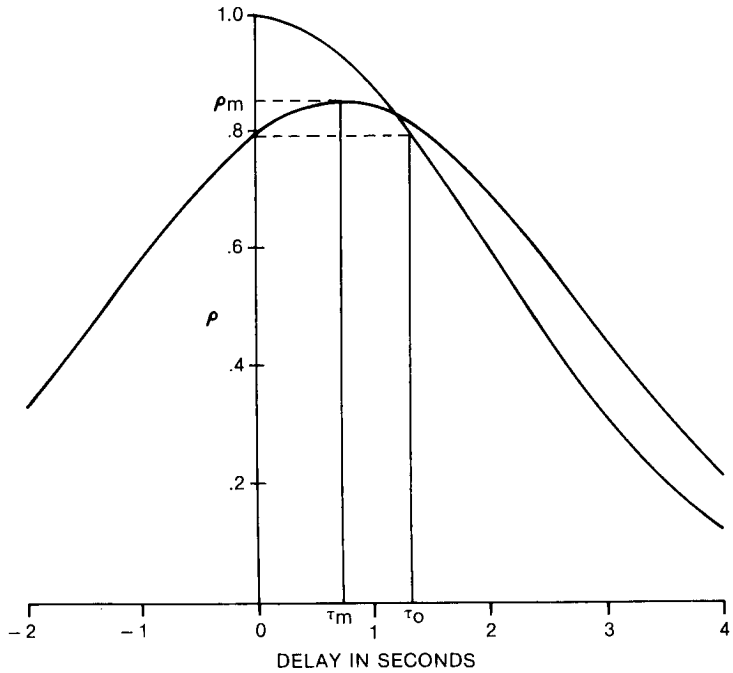

Figure 2.1. Auto-and cross-correlograms for Model 1. $Var(k)^{1/2} = 0.16^0/m$, $Var(\omega)^{1/2} = 20^0/s$, $\sigma = 2.8s$ *and* $r{=}150m$. *The parameters* ρ_m, τ_m *and* τ_0 *are defined in the text.* $Var(k)$ *and* $Var(\omega)$ *are defined in Section 4.*

To derive the coefficient A, Briggs et.al. defined another quantity called the fading velocity(V_f) which is based on the time-delay τ_0 for which the temporal auto-correlation function is equal to the cross-correlation function at zero delay, i.e

$$\rho_{0,\tau_0} = \rho_{r,0}$$

or

$$e^{-\frac{r_0^2}{2\sigma^2}} = e^{-\frac{r^2 A}{2\sigma^2}},$$

i.e.,

$$\begin{aligned} V_f &= r/\tau_0, \\ &= 1/\sqrt{(A)}. \end{aligned} \tag{2.7}$$

Hence,

$$V_d = V_f^2/V_a. \tag{2.8}$$

Briggs et.al. also argued that the temporal random changes in the pattern could be defined in terms of a velocity parameter V_c, where

$$V_f^2 = V_d^2 + V_c^2. \tag{2.9}$$

In extending the method to a two-dimensional case it is considered that a polar coordinate system ($\mathbf{r} = r\ ,\ \theta$) is to be preferred because the correlation function across a random surface, by definition,

is invariant with translation but not with rotation. In an (r, θ) system the correlation function is:

$$\rho_{r,\theta,\tau} = e^{-\frac{r^2(A\cos^2\theta + C\sin^2\theta + N\sin 2\theta) - 2r\tau(H\cos\theta + M\sin\theta) + \tau^2}{2\sigma^2}}, \tag{2.10}$$

where H and M are the reciprocals of the apparent velocity in the x and y directions respectively. The coefficients A, C and N define an ellipse, the correlation ellipse, usually measured for the contour

$$\rho_{r,\theta,0} = 0.5.$$

In the (r, θ) system the above velocity parameters can be defined as a function of θ. Thus,

$$\tau_{m,\theta} = r(H\cos\theta + M\sin\theta), \tag{2.11}$$
$$V_{a,\theta} = 1/(H\cos\theta + M\sin\theta), \tag{2.12}$$
$$\tau_{0,\theta}^2 = r^2(A\cos^2\theta + C\sin^2\theta + N\sin 2\theta), \tag{2.13}$$

and

$$V_{f,\theta}^2 = 1/(A\cos^2\theta + C\sin^2\theta + N\sin 2\theta). \tag{2.14}$$

The direction of the apparent velocity is given by

$$\tan(\phi_a) = M/H. \tag{2.15}$$

The direction of V_d can be derived from the partial derivatives with respect to r and θ of equation 2.10 and can be shown to be

$$\tan(\phi) = (AM - HN)/(HC - MN). \tag{2.16}$$

Then $V_{d,\phi}$ can be derived from

$$V_{d,\phi} = V_{f,\phi}^2/V_{a,\phi}. \tag{2.17}$$

In the application of FCA to the models discussed in this report, a three-antenna system is assumed and a value of τ_m and τ_0 is derived from the correlation functions for each antenna pair. From the three values of τ_m, H and M are derived from a least squares fit to equation 2.11. From the three values of τ_0, A, C and N are derived from 2.13 and the direction of motion ϕ from 2.16. Values of $V_{a,\phi}$ and $V_{f,\phi}$ are derived from 2.12 and 2.14 respectively and hence, $V_{d,\phi}$ from 2.17

The straight line method of Briggs et.al. is based on the time delay τ_a and τ_x for which, for the 1 dimensional case,

$$\rho_{0,\tau_a} = \rho_{r,\tau_x}.$$

From 2.2

$$e^{-\frac{\tau_a^2}{2\sigma_a^2}} = e^{-\frac{Ar^2 - 2Hr\tau_x + \tau_x^2}{2\sigma_x^2}}. \tag{2.18}$$

For reasons that will be explained below, it is assumed here that σ_x(half-width of the cross-correlation function) does not necessarily equal σ_a(half-width of the auto-corelation function). Rearranging the terms of 2.18,

$$\tau_a^2/\sigma_a^2 - \tau_x^2/\sigma_x^2 = Ar^2/\sigma_x^2 - 2Hr\tau_x/\sigma_x^2. \tag{2.19}$$

If $\sigma_a = \sigma_x$, then $(\tau_a^2 - \tau_x^2)$, plotted as a function of τ_x, is a straight line. From the intercept A can be determined and, from the slope, H. However, if $\sigma_a \neq \sigma_x$ then the *straight line* will be curved.

3. SIMILAR FADES ANALYSIS

In similar fades analysis, short sections of pairs of fading records are compared and adjusted in time for best agreement. For the Variant 1 method these delays are averaged and, from the average values, a velocity V_1 is determined in the same manner as for V_a of FCA. This method is also referred to as the average time-delay method.

This particular variant of SFA was originally developed by Mitra(1949) and, over the years, it has been found that the the velocity derived by this method is in very good agreement with the apparent velocity(V_a) of FCA. In the early literature it was frequently referred to as the Mitra method.

For the Variant 2 method a velocity is derived from each set of time-delays per short section using the same method as for V_a and then these velocities are averaged vectorially to produce the Variant 2 velocity V_2. This method is also referred to as the average velocity method.

To clarify possible ambiguity in some of the literature, it should be noted that the results presented by Thomas and Burke(1956), and by Bowman(1968) and referred to as Mitra velocities were actually determined by Variant 2. Those by Burke and Jenkinson(1957) are also from Variant 2.

When the comparison of records is done visually it is customary to select those sections of a record containing only 1 fade and centered around the maximum of this fade. If the pairs of fades are too dissimilar the section is usually rejected. To adapt this process to computer analysis, the auto-correlation coefficients of one record are derived and a value of σ obtained. The records are then divided into lengths of $2\sqrt{(\pi)}\sigma$. This number was derived by Awe(1964) as the statistical distance between maxima in a record. For 4 of the models considered, it was found that the factor of 2 was not too critical. Values of 1.75 to 2.25 could be used without significantly changing the value of the velocities obtained. However, for one model it was found that, if the factor 2 was increased to 4, better agreement between the derived velocity and the true velocity was obtained. This is discussed in the appropriate section. The time-delays between pairs of short sections are derived from cross-correlation analysis analogous to τ_m of FCA. For each set of short sections, if the maximum value of cross-correlation(ρ_m) of any one pair is less than a preset value, that set is rejected. Values of ρ_m between 0.7 and 0.95 are considered and it is found that the best value can vary from model to model. Examples are given with each model.

A further refinement, not used here, is that, for a 3-aerial system, 3 values of time-delays are available but only 2 are needed to find the velocity. Hence, there is 1 degree of freedom and the error in deriving the velocity could be used as a measure to accept or reject that section.

Shown in Figure 3.1 is a sample of fading records derived from Model 1 for a 3-aerial system. The vertical dashed lines indicate the section-breaks dictated by $2\sqrt{(\pi)}\sigma_a$. As can be seen from this figure, better sectioning of the record could be done visually and, from the author's experience, only that fade between 10 and 18 seconds would have been chosen from this sample for finding the time-delays. While better algorithms could be developed for selecting sections, it is considered that such work is outside the scope of this report and only the simple method described above is used here.

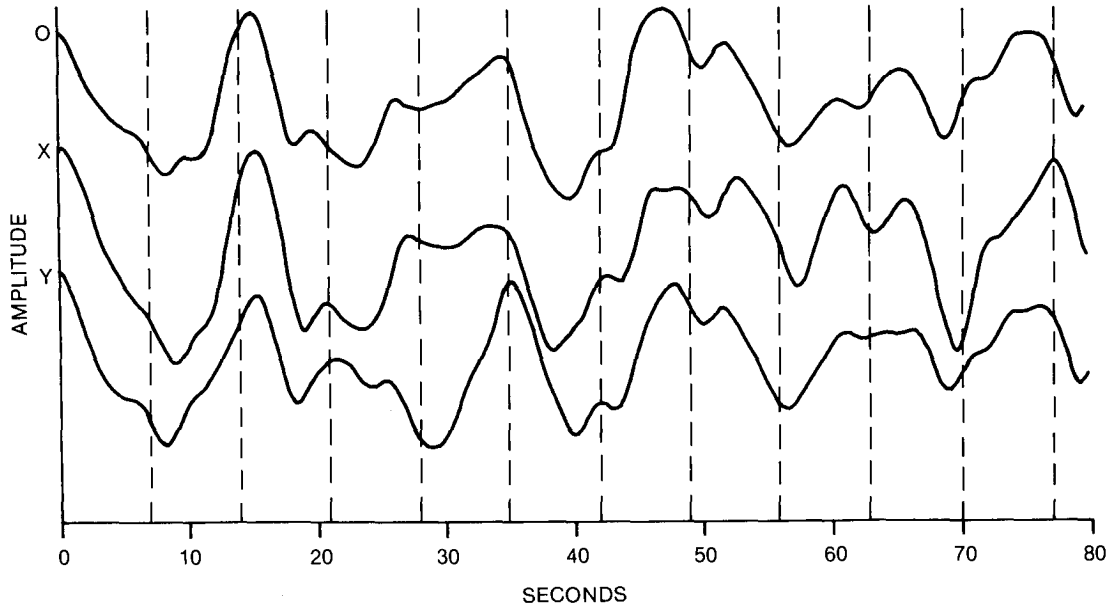

Figure 3.1. Fading records over 80 seconds for Model 1. Design parameters are given by 5.22. The vertical dashed lines define the sections used for SFA and are at $2\sqrt{(\pi)}\sigma_a = 7s$ *intervals.*

4. GENERAL FORM OF RANDOM SURFACES

1.0 INTRODUCTION

In deriving a random surface it is assumed initially that the surface is composed of an infinite set of plane waves all moving with the same speed V and direction ϕ. The amplitude, as a function of space (R, θ) and time t, of a representative wave from this set is given by

$$y_{R,\theta,t} = A_{\omega,k} \cos(\omega t - kR\cos(\phi - \theta) + \epsilon), \tag{4.1}$$

where ω is the angular frequency, k is the wave-number ($= 2\pi/\lambda$, the wavelength), and ϵ is a random phase in the range $(-\pi, \pi)$. There is a particular value of ϵ associated with each wave amplitude $A_{\omega,k}$. R is the distance from the origin. To achieve a Gaussian form for the correlation function it is assumed that

$$A_{\omega,k} = e^{-\frac{\omega^2\sigma^2}{4}}, \tag{4.2}$$

or

$$= e^{-\frac{k^2 s^2}{4}}, \tag{4.3}$$

where s is the half-width of the spatial auto-correlation function. From the above two expressions it follows that

$$\omega/k = s/\sigma, \tag{4.4}$$

and the velocity

$$V = \omega/k. \tag{4.5}$$

The correlation between 2 points, say R and R+r, in the surface is a function of differences, in particular, phase differences. Hence,

$$\begin{aligned} \rho_{r,\theta,\tau} &= \frac{\langle y_{R,\theta,t}\, y_{R+r,\theta,t+\tau}\rangle}{\langle y^2_{R,\theta,t}\rangle}, \\ &= \frac{\langle A^2_{\omega,k} cos(\omega\tau - kr\cos(\phi - \theta))\rangle}{\langle A^2_{\omega,k}\rangle}, \end{aligned} \tag{4.6}$$

where it is assumed that the mean is zero. It will be noticed that the random phase ϵ disappears.

For the ideal surface thus far considered the cross-correlation function will have a maximum value of unity, i.e., perfect correlation. To introduce decorrelation across the surface it follows from 4.6 that there should be random fluctuations in space and/or time of either $A_{\omega,k}$, ω or k or of any combination of these parameters. From the consideration of variations in these parameters 5 models of moving random surfaces are developed. For each surface an analytic solution for the correlation function is derived.

4.2 MODEL 1

This model could be considered as that produced by random phase changes. These phase changes are produced by random changes in velocity from 4.5. Thus the representative wave of 4.1 could be written as

$$y_{R,\theta,t} = A_{\omega,k}\cos(\omega t - R(k_x\cos\theta - k_y\sin\theta) + \epsilon), \tag{4.7}$$

and decorrelation introduced by

$$y_{R,\theta,t} = A_{\omega,k}\cos((\omega+\delta\omega)t - R((k_x+\delta k_x)\cos\theta + (k_y+\delta k_y)\sin\theta) + \epsilon)\ , \tag{4.8}$$

where $k_x = k\cos\phi$ and $k_y = k\sin\phi$ and where δk_x and δk_y are random variables, normally distributed with zero mean, variances $\mathrm{Var}(k_x)$, $\mathrm{Var}(k_y)$ and covariance $\mathrm{Cov}(k_x, k_y)$. Also, $\delta\omega$ is normally distributed with zero mean and variance $\mathrm{Var}(\omega)$. It is assumed in this report that $\delta\omega$ is independent of δk_x and δk_y. It is also assumed, for Model 1, that their variances are independent of ω and k.

It is considered that 4.8 could be better expressed as

$$y_{R,\theta,t} = A_{\omega}\cos(\omega(t - R(H\cos\theta + M\sin\theta)) - R(\delta k_x\cos\theta + \delta k_y\sin\theta) + \delta\omega t + \epsilon), \tag{4.9}$$

where

$$H = k_x/\omega$$

and

$$M = k_y/\omega,$$

and both have the same significance as that for FCA. However it must be stressed that H and M used here are those values for the true velocity (V_t) of the random surface,

$$\text{i.e, } V_t = V = 1/\sqrt{(H^2+M^2)},$$

and are related to the direction of the motion(ϕ) by

$$\tan\phi = M/H.$$

In fact, for the remainder of this report H and M will always have these properties.

It should be noted that, because $\delta\omega$ is assumed independent of δk_x and δk_y, the random surface of 4.8 could be considered as the sum of two surfaces. In one surface, random changes in velocity, magnitude only, are produced by

$$\delta V = \delta\omega/k. \tag{4.10}$$

In the second surface, random changes in reciprocal velocity , both in magnitude and direction, are produced by

$$\delta(1/V) = \delta k/\omega. \tag{4.11}$$

This subject is discussed further in the next section dealing with Model 1.

4.3 MODEL 2

In Model 1 the variances are independent of ω and k, in Model 2 the reverse is true. This effect is achieved through equation 4.9 by defining

$$y_{R,\theta,t} = A_{\omega}\cos(\omega(t(1+\delta\omega/\omega) - R((H+\delta H)\cos\theta + (M+\delta M)\sin\theta)) + \epsilon)\ , \tag{4.12}$$

where $\delta\omega$, δH and δM have the the same properties as that for Model 1 but their variances and covariances are Var(Ω) for $\delta\omega/\omega$ and Var(H), Var(M) and Cov(H, M) for δH and δM.

4.4 MODEL 3

Model 3 is another approach for introducing random phase changes. For this model it is assumed initially that each wave can vary in direction in a random fashion about the true direction of motion, but maintaining a constant speed V. Variations in V are then introduced by way of random frequency changes. For clarity, the wave equation is defined in terms of k rather than ω. Thus

$$y_{R,\theta,t} = A_k \cos(k(R\cos(\phi + \delta\phi - \theta) - Vt) + \delta\omega\, t + \epsilon), \tag{4.13}$$

where $\delta\phi$ is a random variable normally distributed, with zero mean and variance Var(ϕ). $\delta\omega$ is as defined for Model 1.

4.5 MODEL 4

Model 4 is similar to Model 3, except that the variance Var(ω) is a function of k and $\delta\omega/k = \delta V$.

$$y_{R,\theta,t} = A_k \cos(k(R\cos(\phi + \delta\phi - \theta) - (V + \delta V)t) + \epsilon), \tag{4.14}$$

where δV is normally distributed with zero mean and variance Var(V).

4.6 MODEL 5

This model introduces decorrelation by way of random changes in amplitude and not in phase. These changes occur both in space and time. Let

$$D = \delta\alpha + t\,\delta\beta + R(\delta\gamma_x \cos\theta + \delta\gamma_y \sin\theta), \tag{4.15}$$

then

$$y_{R,\theta,t} = A_\omega \cos D \cos(\omega(t - R(H\cos\theta + M\sin\theta)) + \epsilon), \tag{4.16}$$

where $\delta\alpha$, $\delta\beta$ and $\delta\gamma$ are random variables normally distributed with zero mean, variance

$$\text{Var}(\alpha),\ \text{Var}(\beta),\ \text{Var}(\gamma_x),\ \text{Var}(\gamma_y)$$

and the covariances are zero except for Cov(γ_x, γ_y). The variables are independent of ω and k, and $\delta\gamma_x$ and $\delta\gamma_y$ are the random changes in amplitude in the x and y directions, respectively.

As will be shown in Section(9), $\delta\alpha$ is a necessary part of the expression as is ϵ, but plays no part in the correlation function.

5. MODEL 1

5.1 THE CORRELATION FUNCTION

From Section 4 it can be shown that the full correlation function for this model is

$$\rho_{r,\theta\tau} = \frac{\langle \sum_{\omega=0}^{\infty} \sum_{\delta\omega=-\infty}^{\infty} \sum_{\delta k_x=-\infty}^{\infty} \sum_{\delta k_y=-\infty}^{\infty} A_\omega^2 D \rangle}{\langle \sum_{\omega=0}^{\infty} A_\omega^2 \rangle},$$

where

$$D = \cos(\omega(\tau - r(H\cos\theta + M\sin\theta)) - r(\delta k_x \cos\theta + \delta k_y \sin\theta) + \delta\omega\,\tau). \tag{5.1}$$

The general form of the solution of this expression is given by Integral 1 in the Appendix. From this solution it can be shown that

$$\rho_{r,\theta,\tau} = e^{-E} e^{-\frac{(\tau - r(H\cos\theta + M\sin\theta))^2}{2\sigma^2}},$$

where

$$E = \frac{\tau^2 \mathrm{Var}(\omega) + \mathrm{r}^2(\mathrm{Var}(\mathrm{k_x})\cos^2\theta + \mathrm{Cov}(\mathrm{k_x},\mathrm{k_y})\sin 2\theta + \mathrm{Var}(\mathrm{k_y})\sin^2\theta)}{2}, \tag{5.2}$$

and is the same form as 2.10. Thus, it satisfies the conditions for FCA.

From 5.2, the temporal auto-correlation function

$$\rho_{0,0,\tau} = e^{-\frac{\tau^2(1+\sigma^2\mathrm{Var}(\omega))}{2\sigma^2}}, \tag{5.3}$$

$$= e^{-\frac{\tau^2}{2\sigma_a^2}}, \tag{5.4}$$

where

$$\sigma_a^2 = \sigma^2/(1 + \sigma^2\mathrm{Var}(\omega)). \tag{5.5}$$

Because 5.2 is of the same form as 2.10 then $\sigma_a = \sigma_x$. For the Models discussed in this report σ will refer to the input parameter and σ_a and σ_x to the derived values.

Considering the one dimensional case, then 5.2 reduces to

$$\rho_{r,\tau} = e^{-\frac{r^2\mathrm{Var}(\omega)+r^2\mathrm{Var}(\mathrm{k})}{2}} e^{-\frac{(\tau - rH)^2}{2\sigma^2}}. \tag{5.6}$$

From section 2, the various correlation parameters are

$$\tau_m = rH/(1+\sigma^2\mathrm{Var}(\omega)), \tag{5.7}$$
$$V_a = (1+\sigma^2\mathrm{Var}(\omega))/H, \tag{5.8}$$
$$= (1+\sigma^2\mathrm{Var}(\omega))V, \tag{5.9}$$

substituting τ_m for τ in 5.6

$$\rho_m = e^{-\frac{r^2\mathrm{Var}(k)}{2}} e^{-\frac{r^2H^2\mathrm{Var}(\omega)}{2(1+\sigma^2\mathrm{Var}(\omega))}}, \tag{5.10}$$
$$V_f^2 = (1+\sigma^2\mathrm{Var}(\omega))/(H^2+\sigma^2\mathrm{Var}(k)), \tag{5.11}$$

and

$$V_d = H/(H^2+\sigma^2\mathrm{Var}(k)), \tag{5.12}$$
$$= V/(1+V^2\sigma^2\mathrm{Var}(k)). \tag{5.13}$$

As noted in Section 4, V is the true velocity V_t of the surface. It was also noted in Section 4 that the random surface of Model 1 could be considered as the sum of two random surfaces. In one of these surfaces Var(k)=0 and hence, from 5.13, V_d is equal to its true velocity V_t. In the other surface Var(ω)=0 and, from 5.9, V_a is equal to its true velocity. For a combination of these two surfaces, V_t lies somewhere between the values of V_a and V_d derived from this combination. Similar arguments also pertain to the other four models to be considered. It will be noted also from 5.13 that, unless $\mathrm{Var}(k) = 0$, then V_d decreases in value as σ increases. This leads on to the effect of filtering data from the above model before FCA.

5.2 FILTERING

For the above model, using 4.9, series can be readily formed for a multi-antenna system. These series can be developed either in time or space. The effect of filtering time-series before FCA will be considered first and, for simplicity, that for the one-dimensional case.

From 5.12 it follows that, if a time-series is subjected to a high-pass filter before FCA, then the value of V_d obtained will be greater than that from unfiltered data. Conversely, if a low-pass filter is used it will be less.

At first sight, it might be expected from 5.8 that V_a would also be affected by filtering, but this is not so. From 5.1, the frequency terms enter by way of $\omega + \delta\omega$. If these terms are considered as those from a discrete Fourier series then, for the i^{th} harmonic, $(\omega + \delta\omega)$ can be represented as $(i + \delta i)$, where $|\delta i|$ can be greater than one. Let

$$j + \delta j = i + \delta i, \tag{5.14}$$

where j is an integer and $|\delta j| < 1$. Then the amplitude and phase associated with the i^{th} term is moved to the $(j+\delta j)^{th}$ term of the series. If $|\delta j| \neq 0$, this information is *leaked* into the various harmonics on either side of j. Once a time series is formed the information as to where the values of amplitude and phase came from is lost. Thus filtering of a time-series will not affect V_a but it will affect V_d.

It is this movement of harmonic information in the time domain which results in $\sigma_a < \sigma$, as expressed in 5.5. If δi is positive, energy is moved from the lower harmonic i to the higher harmonic j. But, because of the Gaussian nature of the power spectrum, this means that energy is moved from an area where it is relatively high to an area where it is relatively low. The reverse happens if δi is

negative. In the extreme, if Var(ω) is very large, the spectrum of the altered series would approach that of white noise. From 5.5, this movement of energy due to random temporal changes is contained in the term $(1 + \sigma^2 \mathrm{Var}(\omega))$.

This movement of energy from lower to higher frequencies is also accompanied by movement of phase information and, hence, phase differences. If there is no dispersion present, phase difference is a linear function of frequency and the gradient of phase difference versus frequency is inversely proportional to the velocity of the wave components. If phase differences are moved from lower to higher frequencies, the gradient is reduced and the velocity is increased. From 5.8, the effect of random temporal changes is to reduce the gradient by $(1+\sigma^2 \mathrm{Var}(\omega))$, the same factor that reduces σ. It is true that phase differences are also moved from higher to lower frequencies but these are accompanied by less energy than those going the other way.

Since the factor $(1 + \sigma^2 \mathrm{Var}(\omega))$ is imbedded in the data and cannot be recovered by filtering, it follows that ρ_m of 5.10 will be unaffected by filtering.

In the spatial domain the situation is reversed. V_d, which is derived from the spatial delay for maximum spatial cross-correlation, will be unaffected by filtering. On the other hand, V_a will be affected.

This transfer from the i^{th} to the j^{th} harmonic can be used to advantage in terms of reduced computing time for modeling. Time-series can be made for Model 1 by a summation process but, if the the series is a reasonable length, say 1024 values assumed sampled every 0.25 seconds, there will be 512 harmonics to be summed 1024 times. This work can be considerably reduced if a suitable algorithm is used to *leak* the information around the j^{th} term and then using the Fast Fourier Transform to produce the time series. In practice, it was found that, if the necessary information was transferred to 80 harmonics centered on j, the results obtained differed from the summation method by $< 0.5\%$ with a reduction in computing time by a factor of about 12. If less accuracy is acceptable, the time saved can be even greater. The same technique applies to the formation of spatial-series.

5.3 THE LOW-VELOCITY EFFECT

The physical relationships of V_d and V_a can be appreciated if it is assumed two finite time-series from the random surface are recorded a distance r apart in the direction of motion. From the discrete Fourier transform of the series the phase difference, Φ_i for the i^{th} harmonic, can be determined and a value of V_i derived from

$$V_i = 2\pi i r / T \Phi_i.$$

where T is the length of the time-series. The cross-correlation function can then be expressed as

$$\rho_{r,\tau} = \langle \sum_{i=1}^{T/2} A_i^2 \cos \frac{2\pi i}{T}(\tau - \frac{r}{V_i}) \rangle, \tag{5.15}$$

where it is assumed that the normalization term is unity.

The partial derivative of 5.15 with respect to τ for $r = r'$ is

$$\langle \sum_{i=1}^{T/2} A_i^2 \frac{2\pi i}{T} \sin(\frac{2\pi i}{T}(r - \frac{r'}{V_i}) \rangle. \tag{5.16}$$

The value of $\tau = \tau_m$ for which this expression is zero is the necessary condition for $V_a (= r'/r_m)$. If the

sine term is approximated by the first term of its power series, then it can be shown that

$$\frac{1}{V_a} \approx \frac{\langle \sum_{i=1}^{T/2} A_i^2 i^2 / V_i \rangle}{\langle \sum_{i=1}^{T/2} A_i^2 i^2 \rangle}. \tag{5.17}$$

Thus, for this approximation, $1/V_a$ is the weighted sum of $1/V_i$, where the weight is $A_i^2 i^2$. From similar considerations it can be shown that

$$V_d \approx \frac{\langle \sum_{i=1}^{T/2} A_i^2 i^2 V_i / V_i^2 \rangle}{\langle \sum_{i=1}^{T/2} A_i^2 i^2 / V_i^2 \rangle}. \tag{5.18}$$

Hence, V_d is the weighted sum of V_i where the weight is not only proportional to $A_i^2 i^2$,but also to the reciprocal of V_i^2. Low values of V_i will tend to dominate the sum. This effect is referred to as *the low-velocity effect* and the derivation of V_a and V_d from the weighted values of V_i as the weighting method.

If $T = 256s$, $r = 100m$ and $V_i = 100m/s$, the phase difference for the 1^{st} harmonic is 1.4 degrees. If the observed value of $\Phi_i > 1.4^0$ then $V_i < 100m/s$. From 5.1, $r\,\delta k$ comes from a distribution with some reasonable value of $r\mathrm{Var}(k)^{1/2}$, say 10^0 or 20^0, then very low values of V_i are to be expected. On the other hand, if $i = 50$, then, for $V_i = 100m/s$, $\Phi_i = 70^0$ and very low values of V_i will tend to be rare. Hence, filtering out the low frequency components before FCA will result in a higher value of V_d.

It can be shown that, for an infinite series, the weighting function for V_d is given by

$$W_{d,\omega} = e^{\frac{-\omega^2\sigma^2}{2}} r^2(\omega^2 H^2 + \mathrm{Var(k)}) \tag{5.19}$$

and for V_a

$$W_{a,\omega} = e^{\frac{-\omega^2\sigma^2}{2}} \omega^2. \tag{5.20}$$

5.4 FILTERING AND THE LOW-VELOCITY EFFECT FROM MODELING

To test the effect of filtering and the sine approximations made above , sets of time-series for a 3-aerial system were generated. The aerials were assumed to be located at 3 corners of a square of side 100m, with 1 pair of sides in the direction of motion. Each time-series contained 1024 values assumed sampled at 0.25s intervals. The design parameters were;

$$\mathrm{Var(k_x)}^{1/2} = 0.205^0/m, \quad \mathrm{Var(k_y)}^{1/2} = 0.29^0/m, \quad \mathrm{Var}(\omega)^{1/2} = 20^0/s,$$
$$V = 100m/s, \qquad \sigma = 2.8s. \tag{5.21}$$

For convenience the appropriate values are given in degrees rather than radians. For these design parameters the surface is isotropic and the correlation parameters are;

$$V_a = 195m/s, \quad V_d = 49m/s.$$
$$\rho_m = 0.909, \qquad \sigma_a = 2.0s. \tag{5.22}$$

The choice of the particular parameters of 5.21 was dictated by the desire to have V_a about one half, and V_d about twice the true velocity.

In all, 25 sets were formed using a new seed for the random function generator for each set. These sets were analysed by FCA and the vector mean of the 25 sets of V_a and V_d were derived. These means are shown in Table 5.1 for nil filtering. The mean direction obtained was within a few degrees of the designed direction

TABLE 5.1

Model-1.Comparison of V_a and V_d from FCA and weighting method, both before and after filtering. For design parameters and filtering methods see text. All values are in m/s.

FILTER	*FCA*		*WEIGHT*	
	V_a	V_d	V_a	V_d
nil	204	50	208	49
1-10	204	73	212	68
1-20	208	98	217	96
n=4	190	90	224	81

To study the effect of filtering, two methods of producing high-pass filters were used. The first method, a rather simple method, was to delete the first 10 or 20 harmonics from the data before FCA. However, this method changes the shape of the correlation functions and they are no longer Gaussian. On the other hand, this method does show the effect of the low harmonic components on the value of V_d obtained. The second method retains a Gaussian correlation function after filtering and can be set to reduce σ_a from the original series by a given factor. It will be remembered that the amplitudes of the Fourier series had a Gaussian shape given by

$$A_\omega = e^{-\omega^2\sigma^2/4}.$$

If the n^{th} root of A_ω is taken then

$$\sqrt[n]{(A_\omega)} = e^{-\omega^2\sigma^2/4n}. \tag{5.23}$$

Hence, the value of σ after filtering is $\sigma/\sqrt{(n)}$. The velocities obtained after filtering, both by deleting harmonics i=1 to 10 and i=1 to 20, and for n=4, are also included in Table 5.1.

For the weighting method only the pair of time-series in the the direction of motion was considered. These series were Fourier analysed and values of A_i and V_i determined. Values of V_a and V_d were determined by way of 5.17 and 5.18, respectively, and averaged over the 25 sets. The mean values are included in Table 5.1. As can be seen from this Table there is very good agreement between FCA and the weighting method, both for the unfiltered and filtered data. Also, only V_d is effected by filtering.

Using the parameters of 5.21, $W_{d,\omega}$(full line) and $W_{a,\omega}$(dashed line) from 5.19 and 5.20, as a function of ω, are shown in Figure 5.1. Both weights have been normalized to a maximum value of 1. It can be seen that $W_{d,\omega}$ has a much greater weight at the low-frequency end.

In discussing the low-velocity effect, attention was directed towards the phase variations from random spatial changes. However, even if the random spatial changes in the direction of motion are zero and only random temporal changes are considered, the value of V_d will increase after filtering with a high-pass filter. As noted in section 5.2, with $\mathrm{Var}(\omega) \neq 0$ phase information is moved from one harmonic where it is correct to another harmonic where it will be incorrrect. Thus introducing a a phase error

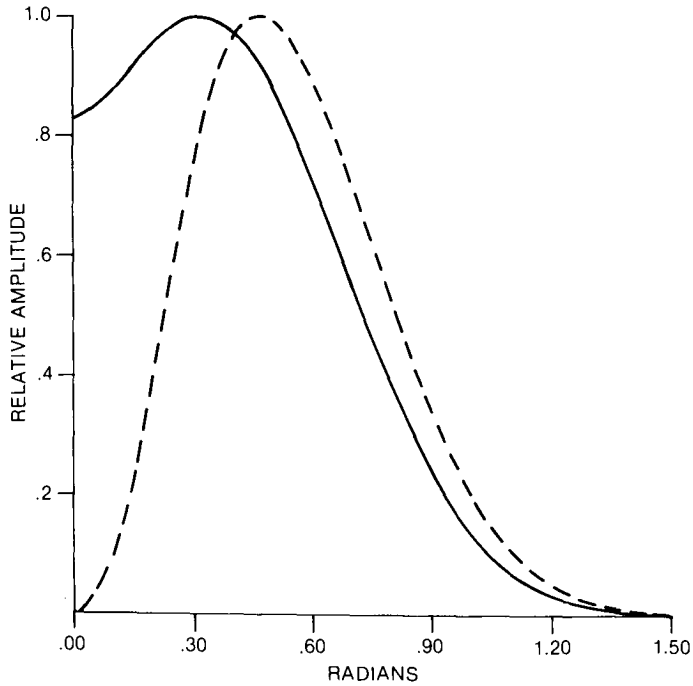

Figure 5.1 Weighting functions for V_d(full line) and V_a(dashed line) as a function of radians.

of $rH\delta\omega$. This effect can best be appreciated by expressing the cross-correlation function of Model 1 in the form

$$\rho_\tau = \rho_m e^{-\frac{(\tau-\tau_m)^2}{2\sigma_a^2}}.$$

From the definition of τ_0, then

$$2\sigma_a^2|\ln\rho_m| + \tau_m^2 = \tau_0^2. \tag{5.24}$$

It has been shown previously that ρ_m and τ_m are independent of filtering, but σ_a does vary with filtering. Hence, from 5.24, τ_0 and thus V_f will vary with filtering. It follows V_d will likewise vary. Chandra and Briggs(1978) arrived at the same conclusion from a slightly different line of reasoning. However, it will be noted from 5.24 that the filter effect is a function of ρ_m and that, from 5.10, ρ_m is a function of Var(k) and Var(ω).

To show the effect of Var(ω), the work on filtering was repeated with the design parameters of 5.21 except that Var(k_x) = 0.The results are shown in Table 5.2.

TABLE 5.2

Various correlation parameters derived from data for Model 1 before and after filtering. The design parameters are as in 5.21, except Var(k_x) = 0.

FILTER	V_a	V_d	ρ_m
nil	205	96	.97
$i = 1-10$	205	121	.97
$i = 1-20$	203	145	.97

5.5 SIMILAR FADES ANALYSIS

The time-series used for obtaining the results shown in Table 5.1 were subjected to similar fades analysis for various levels of ρ_m for acceptance. The results are shown in Table 5.3. The percentage of sections accepted are also shown in the Table. Section lengths of $2\sqrt{(\pi)}\sigma_a$ seconds were used for this work.

TABLE 5.3

Values of V_1 and V_2 from SFA for various levels of ρ_m. The design parameters are as in 5.21.

ρ_m	*%Sections*	V_1	V_2
.75	74	222	101
.80	71	222	102
.85	68	216	103
.90	63	214	106
.95	53	213	115

These values are in good agreement with the expected values of 195m/s and 100m/s for the random surface and are relatively independent of the level of ρ_m used.

5.6 THE CORRELATION ELLIPSE

From 5.2, the contours of constant correlation which define the correlation ellipse are given by

$$2\sigma_a^2|\ln \rho_{r,\theta,0}| = r^2((II^2 + \sigma^2 \mathrm{Var}(\mathrm{k_x}))\cos^2\theta + (\mathrm{MII} + \sigma^2 \mathrm{Cov}(\mathrm{k_x}, \mathrm{k_y}))\sin 2\theta + (M^2 + \sigma^2 \mathrm{Var}(\mathrm{k_y}))\sin^2\theta). \quad (5.25)$$

If the variances of this expression are zero, i.e., no spatial changes, the ellipse will have an axial ratio of ∞. If the covariance is not zero, the ellipse will be oriented with neither of its axis in the direction of motion.

To compare the theoretical correlation ellipse with the shape of individual patterns in the random surface, modeling was carried out by simulating an 11×11 aerial array, with 100m spacing between aerials. The design parameters were as given in 5.21. From these amplitude patterns, correlation ellipses were derived by the method developed by Felgate and Golley(1971). These workers were recording on an 89 aerial array, roughly circular, with a diameter of 1km.

An example of the type of amplitude patterns obtained is shown in Figure 5.2, where, for convenience, the amplitude has been normalized to lie in the range 0 to 10 units. For detail in plotting, the amplitudes for this plot were derived at 25 m spacing. Also included in the Figure is the correlation ellipse derived for a value of $\rho(r, \theta, 0) = 0.5$. The direction of motion of the surface is towards the right.

Another pattern is shown in Figure 5.3, this pattern was derived 10s after that for Figure 5.2 using the same set of random variables. As can be seen, the axial ratio of the correlation ellipse can change dramatically in a period of 10s from 1.34 in Figure 5.2 to 2.38 in Figure 5.3. Also, it will be noted that the area of the ellipse can also change just as dramatically.

To investigate the spread in axial ratios, 150 patterns were derived in 6 sets of 25. For each set a new range of random variables was used and, within a set, the same range of random variables was used

to generate patterns at intervals of 10 seconds. For these 150 samples, the axial ratio varied from 1.0 to 2.66, with a median value of 1.46 and a 95 percentile value of 2.19. These results are not inconsistent with the arguments of Burke(1975) that the correlation ellipse is the average of the shapes within a random pattern. However, it should be noted that, if the theoretical ellipse has a high axial ratio, then individual patterns will also have a high value of axial ratio i.e., fringe-like, with each pattern oriented close to the orientation of the theoretical ellipse. In practice, this situation will occur for orientation of the major axis at right angles to the direction of motion for which direction the random spatial changes will be negligeable.

In conclusion, it can be seen for Model 1, that special conditions are needed if FCA is to provide a true value of speed of the random surface. These condition are that, while random temporal changes are permitted, there must be no random spatial changes in the direction of motion. However, if the axial ratio of the correlation ellipse is to be finite, then there must be random spatial changes at right angles to the direction of motion. These conditions are considered to be very restrictive and unrealistic. Moreover the ellipse will always be oriented with one of its axis in the the direction of motion.

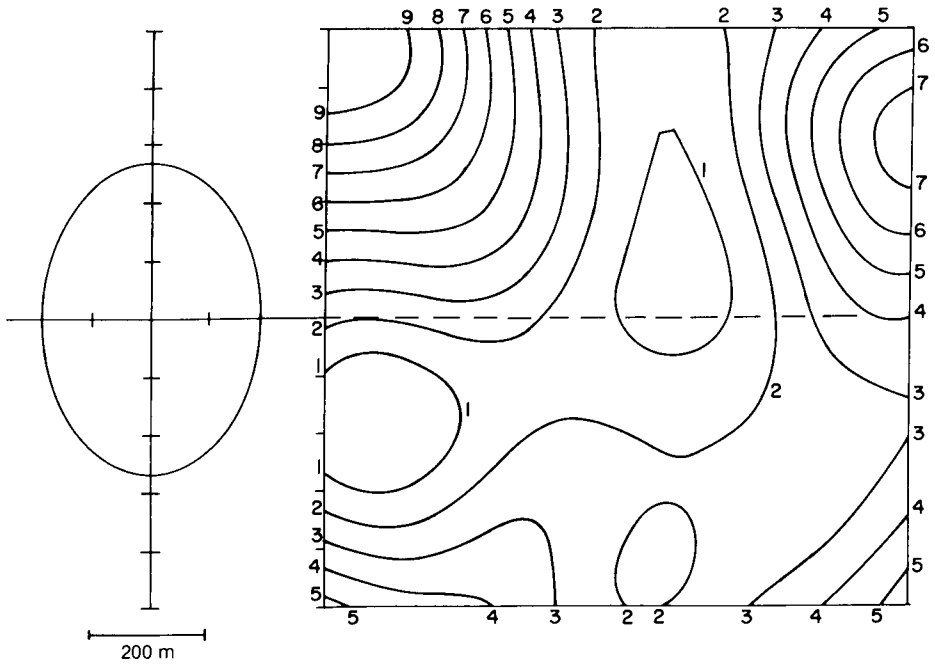

Figure 5.2 Contours of constant amplitude over a 1 × 1 km area for Model 1. The design parameters are defined in 5.21. The correlation ellipse has an axial ratio of 1.36.

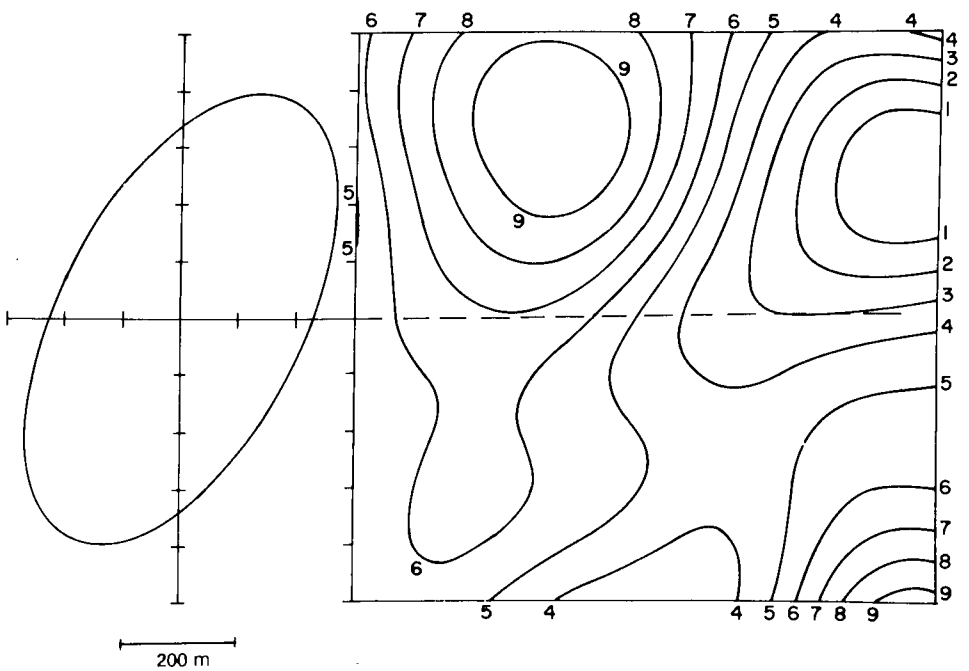

Figure 5.3 *As for Figure 5.2, except that it is 10 seconds later. The correlation ellipse axial ratio is 2.05.*

6. MODEL 2

6.1 THE CORRELATION FUNCTION

From Section 4 it can be shown that the correlation function for this model is

$$\rho_{r,\theta,\tau} = \frac{\langle \sum_{\omega=0}^{\infty} \sum_{\delta\Omega=-\infty}^{\infty} \sum_{\delta H=-\infty}^{\infty} \sum_{\delta M=-\infty}^{\infty} A_\omega^2 D \rangle}{\langle \sum_{\omega=0}^{\infty} A^2(\omega) \rangle},$$

where

$$D = \cos\omega((1+\delta\Omega)\tau - r((H+\delta H)\cos\theta + (M+\delta M)\sin\theta). \tag{6.1}$$

The general form of the solution of this expression is given by Integral 2 in the Appendix. From this solution it can be shown that

$$\rho_{r,\theta,\tau} = E^{-\frac{1}{2}} e^{-\frac{(\tau - r(H\cos\theta + M\sin\theta))^2}{2\sigma^2 E}},$$

where

$$E = 1 + \frac{\tau^2 \mathrm{Var}(\Omega) + r^2(\mathrm{Var}(H)\cos^2\theta + \mathrm{Cov}(H,M)\sin 2\theta + \mathrm{Var(M)}\sin^2\theta}{\sigma^2}, \tag{6.2}$$

and the variances are as defined in section 4.

The presence of $E^{-\frac{1}{2}}$ in 6.2 indicates that the correlation function will not be Gaussian. However, if $\rho_{r,\theta,r}$ is greater than about 0.8, then, to a good approximation(-3%),

$$E^{-\frac{1}{2}} \approx e^{-\frac{(E-1)}{2}}. \tag{6.3}$$

For the one-dimensional case, with the above approximation, 6.2 can be expressed as

$$\rho_{r,\tau} = e^{-\frac{r^2\mathrm{Var}(\Omega) + r^2\mathrm{Var}(H)}{2\sigma^2}} e^{-\frac{(\tau - rH)^2}{2\sigma^2 E}}, \tag{6.4}$$

which does have a Gaussian form. From modeling, it has been found that, for $r = 100m$ and $\sigma > 2.0s$, the approximation is reasonable. From 6.4 it, can be seen that, although both the temporal auto- and cross-correlation functions will have a Gaussian form, $\sigma_x > \sigma_a$ and that the ratio σ_x/σ_a will increase with increasing r.

Another way of viewing this is to let $\mathrm{Var}(\Omega) = 0$, in which case 6.2, for the one-dimensional case, can be written as

$$\rho_{r,\tau} = \rho_m e^{-\frac{(\tau - rH)^2}{2\sigma^2/\rho_m^2}}, \tag{6.5}$$

where

$$\rho_m = 1/(1 + r^2 \mathrm{Var}(H)/2\sigma^2)^{1/2} . \tag{6.6}$$

It should be noted that ρ_m should be expressed as a function of r, i.e., $\rho_m(r)$. Thus

$$\sigma_x = \sigma_a/\rho_m(r). \tag{6.7}$$

Because σ_x is greater than σ_a and is a function of aerial spacing, this model does not conform to the basic assumptions required for FCA. Thus, if the straight-line method of Briggs et.al. is applied to data from this model the *straight line* of the straight-line method will not be straight. However, if FCA is applied to the data to find V_a and V_f, certain distinctive features appear which are contrary to those of Model 1.

Because σ_x increases with r, then τ_0 of Section 2 used for finding V_f does not increase linearly with r as for Model 1. Rather, its value is less than that expected from the linear relationship. Hence, V_f will increase with r and likewise V_d which is derived from V_f^2/V_a. Because $\mathrm{Var}(\Omega) = 0$ for this discussion, then V_a remains unchanged. With $\mathrm{Var}(\Omega) \neq 0$, the conclusions that V_f and V_d increase with r remain essentially the same but the reasons are not as obvious.

The increase of V_d and the ratio of σ_x/σ_a, as a function of r for various values of $\mathrm{Var}(\Omega)$, are shown in Table 6.1 for $V = 100m/s$ and $\mathrm{Var}(H)^{1/2} = H(1/V)$. It should be remembered that, for this Model, V is the true velocity of the random surface. Values of σ were chosen so that σ_a was always 2s. σ_x^- and σ_x^+ refer to the values of σ to the left and right of ρ_m, respectively. As can be seen from the Table, the effect is more pronounced for low values of $\mathrm{Var}(\Omega)$. This could be due to the fact that the values of σ_x are asymmetric with high values of $\mathrm{Var}(\Omega)$ and it is the negative values that affect τ_0.

TABLE 6.1

V_a, V_d and σ_x/σ_a as a function of r and $\mathrm{Var}(\Omega)$.For design parameters see text.

		$r = 100m$				$r = 200m$			
$\mathrm{Var}(\Omega)^{1/2}$	σ	V_a	V_d	σ_x^-/σ_a	σ_x^+/σ_a	V_a	V_d	σ_x^-/σ_a	σ_x^+/σ_a
0.00	2.00	100	59	1.12	1.12	100	83	1.41	1.41
0.25	2.00	106	57	1.10	1.15	106	78	1.38	1.49
0.50	2.03	124	54	1.05	1.20	124	55	1.29	1.59
1.00	2.30	196	50	1.03	1.17	191	52	1.20	1.52

6.2 FILTERING

From a comparison of the correlation parameters obtained from data derived for Model 2, both before and after filtering it was found that the results were essentially the same as for Model 1, except that ρ_m was affected by filtering. It increased after low-pass filtering and decreased with high-pass.

To show this effect, modeling was carried out as described for Model 1, where 25 sets of 3-aerial time-series were subjected to FCA both before and after the use of a high-pass filter. The design parameters used were

$$\begin{aligned} \mathrm{Var}(H)^{1/2} &= H, & \mathrm{Var}(M)^{1/2} &= 1.53H, & \mathrm{Var}(\Omega)^{1/2} &= 1, \\ V &= 100m/s, & \sigma &= 2.3s. \end{aligned} \tag{6.8}$$

The motion of the surface was in the x direction for which H=1/V and M=0 s/m. For this direction, it was found convenient to define Var(H) and Var(M) in terms of H. For the above conditions the correlation parameters were computed to be;

$$\begin{aligned} V_a &= 196 m/s, & V_d &= 50 m/s, \\ \rho_m &= 0.88, & \sigma_a &= 2.0 s, \end{aligned} \tag{6.9}$$

where ρ_m is that from the pair of time-series in the direction of motion. Filtering was carried out by the two methods used for Model 1, i.e., deleting harmonics from the beginning of the series or by reducing the harmonic amplitudes appropriately. However, for Model 2 it was found that a factor of n=2 was sufficient to halve the value of σ, no doubt because of the non-Gaussian shape of the correlation functions. The results from before and after filtering are shown in Table 6.2. As can be seen, the effect of filtering is as described above.

TABLE 6.2

Various correlation parameters derived from data for Model 2 before and after high-pass filtering.The design parameters are as in 6.8.

FILTER	V_a	V_d	ρ_m
nil	220	56	.88
$i = 1 - 10$	219	70	.84
$i = 1 - 20$	230	86	.82
$n = 2$	217	80	.81

It was also found that the weighting method worked as well for this Model as for Model 1. Values of 235 and 40 m/s were found for V_a and V_d respectively.

To show the effect of filtering on data where there are no random spatial changes in the direction of motion, the work on filtering was repeated with the design parameters of 6.8 except that Var(H) = 0.The results are shown in Table 6.3.

TABLE 6.3

Various correlation parameters derived from data for Model 2 before and after filtering.The design parameters are as in 6.8, except that Var(H)=0.

FILTER	V_a	V_d	ρ_m
nil	204	95	.95
$i = 1 - 10$	203	125	.95
$i = 1 - 20$	210	149	.95

The interesting feature of the above results is that ρ_m is unchanged after filtering. Whereas, from Table 6.2, when random spatial changes are present ρ_m is reduced.

6.3 SIMILAR FADES ANALYSIS

The data used for filtering were also used for SFA. The mean values of V_1 and V_2 obtained are shown in Table 6.4. While V_1 is a little high, V_2 is in fair agreement with the true velocity of 100m/s, especially for low levels of ρ_m.

TABLE 6.4

Values of V_1 and V_2 derived with SFA for various levels of ρ_m. The design parameters are as in 6.8.

ρ_m	$\%Sections$	V_1	V_2
.70	58	245	95
.75	55	241	106
.80	48	242	111
.85	40	238	116
.90	30	244	124

6.4 THE CORRELATION ELLIPSE

Because the shape of the correlation function of Model 2 is only approximately Gaussian then, for a particular design, the axial ratio of the correlation ellipse will vary slightly for different levels of contours of constant correlation. This effect can be seen from the variation of V_f with increasing r. As noted in Section 2, V_f defines the correlation ellipse. From the work used for producing Table 6.1, the variation of V_f with r is shown in Table 6.5.

TABLE 6.5

V_f as a function of r for various values of Var(Ω). *The design parameters are as used for Table 6.1.*

$\mathrm{Var}\Omega^{1/2}$	$r = 100m$	$r = 200m$
0.00	77	91
0.25	78	91
0.50	82	83
1.00	99	100

It will be noted from this Table that the greatest increase in V_f occurs with Var(Ω) = 0. If V_f increases with r, then the correlation ellipse will tend to be oriented with its major axis in the direction of the antenna pair with the greatest spacing. For consistency, the level for $\rho = 0.5$ will be used for defining the ellipse for the work presented below.

As for Model 1, various sets of data were generated for an 11×11 aerial array with 100m spacings and the correlation ellipse computed for each pattern. The design parameters were as in 6.8. For these conditions the surface is isotropic. For the 150 ellipses computed, the axial ratio varied from 1.04 to 2.52, with a median value of 1.40 and a 95 percentile of 2.07. Amplitude patterns 10 seconds apart are shown in Figures 6.1 and 6.2, with their corresponding ellipses.

Overall, the results are the same as for Model 1, except that there is finer detail structure in the contours of constant amplitude for Model 2 than for Model 1. It is considered that this occurs because Var(H) and Var(M) are a function of σ and , hence, of the frequency components of the pattern.

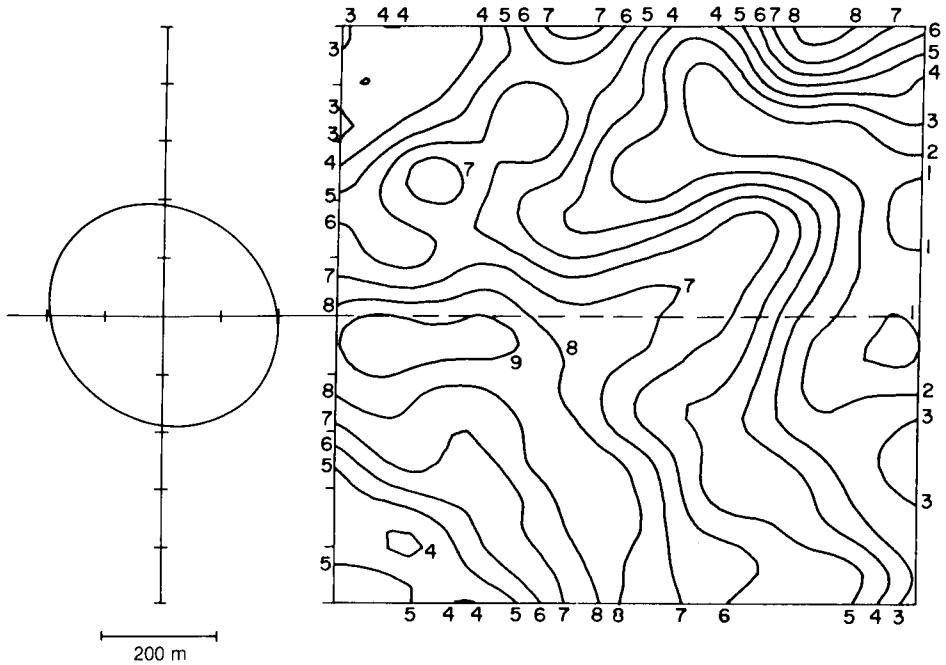

Figure 6.1 Contours of constant amplitude over a 1 × 1 km area for Model 2. The design parameters are defined in 6.8. The correlation ellipse has an axial ratio of 1.1.

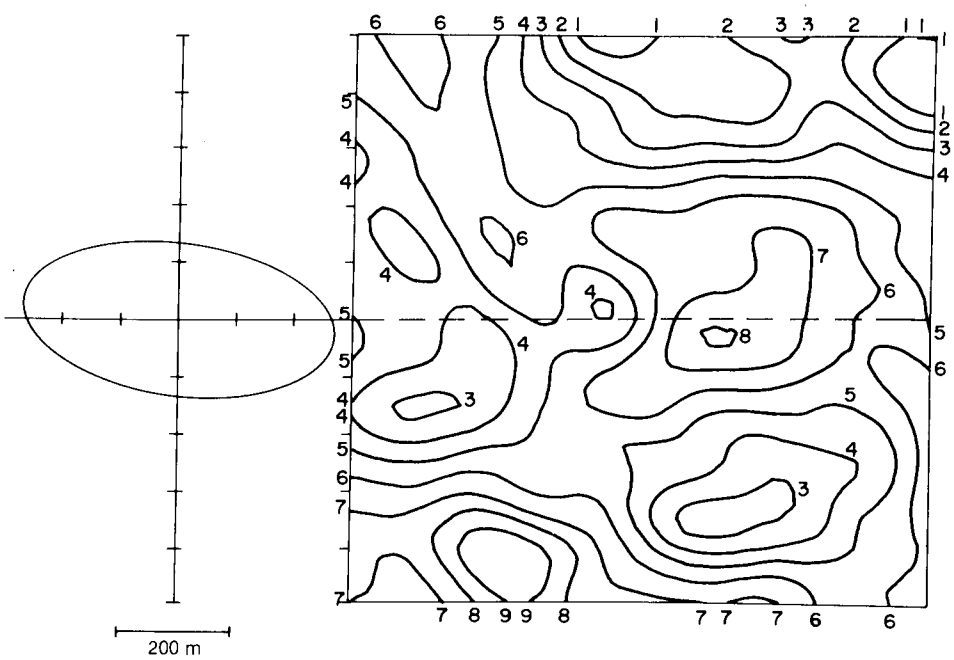

Figure 6.2 As for Figure 6.1, except that it is 10 seconds later. The correlation ellipse axial ratio is 1.98.

7. MODEL 3

7.1 THE CORRELATION FUNCTION

From Section 4 the correlation function for this model is

$$\rho_{r,\theta,\tau} = \frac{\left\langle \sum_{k=0}^{\infty} \sum_{\delta\phi=-\infty}^{\infty} \sum_{\delta\omega=-\infty}^{\infty} A_k^2 \cos(k(r\cos(\phi+\delta\phi+\theta) - V\tau) - \delta\omega\tau) \right\rangle}{\left\langle \sum_{k=0}^{\infty} A_k^2 \right\rangle}. \tag{7.1}$$

The solution for 7.1 is given by Integral 3 in the Appendix, i.e.,

$$\rho_{r,\theta,\tau} = e^{-\frac{\tau^2 \mathrm{Var}(\omega)}{2}}(D+E),$$

where

$$\begin{aligned}
D &= \sum_{n=0}^{\infty} q \cos\frac{n\pi}{2} e^{-\frac{n^2\mathrm{Var}(\phi)}{2}} \cos n(\phi+\theta)\, C_m, \\
E &= \sum_{n=0}^{\infty} \sin\frac{n\pi}{2} e^{-\frac{n^2\mathrm{Var}(\phi)}{2}} \cos n(\phi+\theta)\, S_m, \\
C_m &= \sum_{m=0}^{\infty} \cos\frac{m\pi}{2} \frac{r^{n+2m}}{2^{n+2m} m!(n+m)!} \sum_{p=0}^{\infty} \cos\frac{p\pi}{2} \frac{(V\tau)^p}{p!} \frac{1^{\frac{n+2m+p}{2}:2}}{s^{n+2m+p}}, \\
S_m &= \sum_{m=0}^{\infty} \cos\frac{m\pi}{2} \frac{r^{n+2m}}{2^{n+2m} m!(n+m)!} \sum_{p=0}^{\infty} \sin\frac{p\pi}{2} \frac{(V\tau)^p}{p!} \frac{1^{\frac{n+2m+p}{2}:2}}{s^{n+2m+p}},
\end{aligned} \tag{7.2}$$

$q = 1$ for $n = 0$; else $q = 2$. and $1^{\frac{n+2m+p}{2}:2}$ is in Kramps's notation.

This solution was determined from working in the k-domain. It can also be readily determined from the ω-domain by using

$$A_\omega^2 \cos(\omega(\tau - \frac{r}{V}\cos(\phi+\delta\phi-\theta)) + \delta\omega\tau) \tag{7.3}$$

in 7.1 and summing with respect to ω. The only change in 7.2 is to replace s with $V\sigma$. An other way is to replace s with σ, $V\tau$ with τ and r with r/V. It should be noted that random spatial changes for this model enter by way of $\mathrm{Var}(\phi)$.

7.2 SURFACE SPEED

For this model the speed of the random surface will be greater than V. This can be seen from 7.3 if $\mathrm{Var}(\omega) = 0$ and $\phi = \theta = 0$, i.e.,

$$A_\omega^2 \cos(\omega(\tau - \frac{r\cos\delta\phi}{V})). \tag{7.4}$$

To the first approximation, the true speed,V_t, of the surface is given by

$$1/V_t \approx \langle \cos\delta\phi \rangle / V. \tag{7.5}$$

This is based on the assumption that, for $\mathrm{Var}(\omega) = 0$, the speed of the surface is given by V_a from FCA.

From Bierens de Haan(1939),Tables 29.2 and 263.6, the integrals of

$$\int_0^\infty e^{-px^2} dx = 0.5\sqrt{(\pi/p)} \tag{7.6a}$$

and

$$\int_0^\infty e^{-px^2} \cos qx\, dx = 0.5e^{-\frac{q^2}{4p}} \sqrt{(\pi/p)}. \tag{7.6b}$$

Using these integrals it can be shown that

$$\langle \cos\delta\phi \rangle = e^{-\frac{\mathrm{Var}(\phi)}{2}}. \tag{7.7}$$

Hence,

$$V_t \approx V e^{\frac{\mathrm{Var}(\phi)}{2}}. \tag{7.8}$$

This assumption does not take into account the summation over ω. Hence, to a certain extent, V_t will also be a function of σ.

The degree of goodness of the above approximation is shown in Table 7.1. The results presented there were obtained by generating sets of correlation coefficients from 7.2 for various values of $\mathrm{Var}(\phi)$ and σ, with $V = 100m/s$, $r = 100m$ and $\mathrm{Var}(\omega) = 0$. The correlograms were then subjected to FCA and the values of V_a, V_d, ρ_m, σ_x^-/σ_a and σ_x^+/σ_a obtained are as given in Table 7.1. To assess the degree of goodness of the approximation of 7.8, all values of V_a were multiplied by the appropriate value of $e^{-\mathrm{Var}(\phi)/2}$ and the results are given in parenthesis. The expected value is 100m/s and, to the extent that the computed values differ from 100m/s, is the degree of goodness of the approximation. As can be seen from the Table, the approximation is best for low values of $\mathrm{Var}(\phi)$ and high values of σ. The values of V_d were also scaled down by the same factor as for V_a and the reduced values included in parenthesis. As can be seen, V_d decreases with increasing $\mathrm{Var}(\phi)$. This is consistent with the results of the previous models since the random spatial changes increase in magnitude with increasing $\mathrm{Var}(\phi)$.

Although the values shown in Table 7.1 are for $r = 100m$, the same values can be also used to show the variation of the correlation parameters with r. This occurs because the values are constant for a given ratio of r/σ(for a givenVar(ϕ)). Thus, for a given $\mathrm{Var}(\phi)$, the values of V_a, etc. at $r = 100m$ and $\sigma = 1s$ are the same as for $r = 200m$ and $\sigma = 2s$. On this basis, it can be seen that there is a slight reduction in V_a and hence V_t with increasing r. Also, V_d and the ratios of σ_x/σ_a increase with increasing r.

The values of σ_x/σ_a in Table 7.1 are for $\mathrm{Var}(\omega) = 0$. The effect of $\mathrm{Var}(\omega) \neq 0$ is shown in Table 7.2 for $r = 100m$ and $r = 200m$ with $\mathrm{Var}(\phi)^{1/2} = 65^0$. For convenience, all values of V_a and V_d are expressed as a percentage of V_t found for $\mathrm{Var}(\omega) = 0$ at $r = 100m$.

TABLE 7.1

Variation in parameters from FCA of the correlation function of 7.2. $V = 100m/s$, $r = 100m$ *and* $\mathrm{Var}(\omega) = 0$.

$\mathrm{Var}(\phi)^{1/2}$	σ	V_a	V_d	ρ_m	σ_x^-/σ_a	σ_x^+/σ_a
30	1	114(99)	113(99)	.987	1.01	1.01
30	2	115(100)	110(96)	.996	1.00	1.00
30	4	115(100)	110(96)	.998	1.00	1.00
45	1	131(96)	122(90)	.955	1.04	1.01
45	2	135(99)	114(84)	.987	1.01	1.01
45	4	135(99)	115(84)	.997	1.00	1.00
60	1	156(90)	122(71)	.911	1.11	1.07
60	2	168(97)	108(62)	.974	1.03	1.02
60	4	172(99)	105(61)	.993	1.01	1.01
90	1	254(74)	82(24)	.831	1.26	1.17
90	2	318(93)	63(18)	.950	1.06	1.05
90	4	337(98)	59(17)	.987	1.01	1.01
135	1	1041(65)	20(1)	.793	1.31	1.28
135	2	1458(91)	14(.9)	.941	1.06	1.06
135	4	1586(98)	13(.8)	.985	1.02	1.02

TABLE 7.2

Various correlation parameters as a function of $\mathrm{Var}(\omega)$ *and* r *for* $\mathrm{Var}(\phi)^{1/2} = 65^0$ *and* $\sigma = 2s$.

	$r = 100m$				$r = 200m$			
$\mathrm{Var}(\omega)^{1/2}$	$\%V_a$	$\%V_d$	σ_x^-/σ_a	σ_x^+/σ_a	$\%V_a$	$\%V_d$	σ_x^-/σ_a	σ_x^+/σ_a
0	100	56	1.04	1.03	91	64	1.14	1.08
10	113	55	1.03	1.03	105	63	1.12	1.08
20	152	54	1.02	1.02	146	60	1.10	1.07

Overall, independent of $\mathrm{Var}(\omega)$, V_a tends to decrease with increasing r whereas, V_d and σ_x/σ_a tend to increase. However, for a given r, as $\mathrm{Var}(\omega)$ increases the ratio of σ_x/σ_a tends to decrease. This latter effect is consistent with that found for Model 2, as shown in Table 6.1. On the other hand, from a comparison of the values in Tables 6.1 and 7.2, it will be noted that ratios are not as great with Model 3 as Model 2, nor is the change in V_d.

7.3 FILTERING

To study the effect of high-pass filtering on data from this model, 25 sets of of time-series were generated as described in Section 5.2. The design parameters were

$$\begin{aligned} \mathrm{Var}(\phi)^{1/2} &= 65^0, & \mathrm{Var}(\omega)^{1/2} &= 17^0/s, \\ V &= 100m/s, & \sigma &= 2.5s. \end{aligned} \tag{7.9}$$

For these parameters, the axial ratio of the correlation ellipse is 1.1, $V_t = 183m/s$ and $\sigma_a = 2s$. The value of $\mathrm{Var}(\phi)^{1/2} = 65^0$ was chosen because it was found from modeling with values of Var(H) and Var(M) of 6.8, that the standard deviation of ϕ was about 65^0.

The mean values of V_a and V_d obtained before and after filtering are shown in Table 7.3, expressed

as a percentage of V_t. The value of n=4 was used because, for this value, σ_a was reduced from a mean value of 1.99 to 1.03. This indicates that the correlograms are approximately Gaussian. For reference, a plot of the temporal correlograms for the above design parameters and for $r = 200m$ is shown in Figure 7.1. The dashed curve is for the cross-correlogram at right angles to the direction of motion.

TABLE 7.3

Comparison of V_a and V_d before and after the use of a high-pass filter. The design parameters are as in 7.9.

FILTER	$\%V_a$	$\%V_d$	ρ_m
nil	156	51	.968
1 – 10	155	60	.961
1 – 20	157	64	.946
$n = 4$	145	64	.912

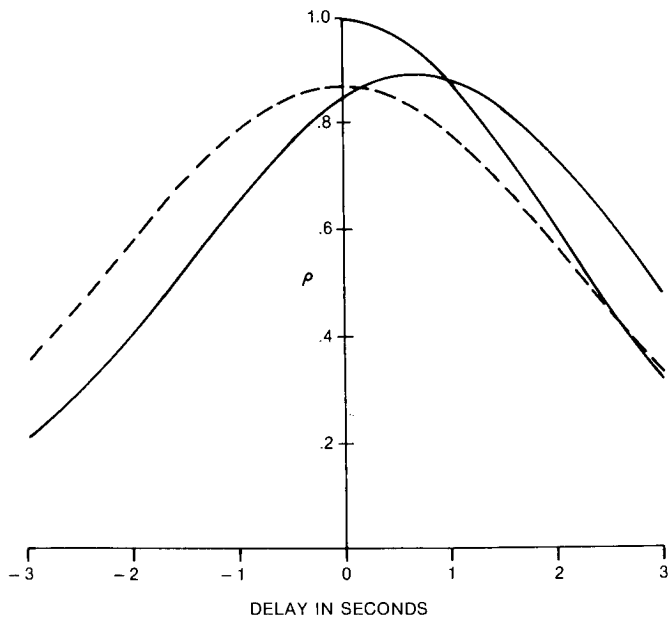

Figure 7.1 Auto- and cross-correlograms for Model 3. The design parameters are defined in 7.9. The dashed line is for the cross-correlogram at right angles to the direction of motion.

From a comparison of the values in Table 7.2 with those in Table 6.1, it will be noted that filtering does not affect V_d for Model 3 as much as it does for Model 2. On the other hand, from use of the weighting method, mean values of 142% and 49% were obtained for V_a and V_d, respectively. These compare favourably with the unfiltered values of Table 7.2. Thus, the low-velocity effect is present but its effect is not as great.

7.4 SIMILAR FADES ANALYSIS

The data used in the previous section were also subjected to SFA. The results obtained from the various levels of acceptance determined by ρ_m are shown in Table 7.4 where, as for Table 7.3, the

velocities are expressed as a percentage of V_t. It will be noted that V_1 is in good agreement with the unfiltered value of V_a of Table 7.2 but V_2, while a better estimate of V_t than V_d, is still somewhat low.

TABLE 7.4

Values of V_1 and V_2 from SFA as a function of ρ_m. The design parameters are as in 7.9. The values are expressed as a percentage of V_t at r=100m.

ρ_m	$\%Sections$	$\%V_1$	$\%V_2$
.75	82	155	77
.80	82	154	77
.85	79	153	78
.90	74	150	83
.95	63	152	86
.975	50	152	88

The values in Table 7.4 were derived for section lengths of $2\sqrt{(\pi)}\sigma$ seconds. It was found that for this model, if the section lengths were increased, then values of V_2 closer to V_t were obtained. This effect is shown in Table 7.5 for section lengths of $M\sqrt{(\pi)}\sigma$ seconds, where M is varied from 2 to 4.

TABLE 7.5

Effect of different section lengths for SFA. $\rho_m = 0.85$.

M	$\%Sections$	$\%V_1$	$\%V_2$
2.0	79	153	78
2.5	80	153	90
3.0	80	152	93
4.0	84	154	106

7.5 CORRELATION ELLIPSE

Analogous to Model 2, because $\sigma_x > \sigma_a$, V_f will vary with r. This variation is shown in Table 7.6. The values were obtained for the same design parameters as used for the results of Table 7.2

TABLE 7.6

V_f as a function of r for various values of $\mathrm{Var}(\omega)$ *.The values are expressed as a percentage of V_t at r=100m. The design parameters are as in 7.9, except for the variation of* $\mathrm{Var}(\omega)$.

$\mathrm{Var}(\omega)^{1/2}$	$r = 100m$	$r = 200m$
0	75	76
10	79	81
20	91	94

It will be noted from this Table that, compared with Model 2, the changes are relatively small. This occurs because V_t tends to decrease with r. For the work presented below the correlation ellipse is defined for $\rho = 0.5$.

From the the way in which the random surface is formed for Model 3 ,the correlation ellipse will always be oriented with its major axis at right angles to the direction of motion and its axial ratio as a function of $\mathrm{Var}(\phi)$. This variation with $\mathrm{Var}(\phi)$ is shown in Table 7.7. These values were computed from 7.2 and are independent of the value of σ used. As can be seen from the Table, the axial ratio varies monotonically from ∞ to 1 as $\mathrm{Var}(\phi)^{1/2}$ increases from 0^0

TABLE 7.7

Axial ratio of correlation ellipse at $\rho = 0.5$ *as a function of* $\mathrm{Var}(\phi)$.

$\mathrm{Var}(\phi)^{1/2}$	Axial ratio
15	3.9
30	2.3
45	1.4
60	1.2
90	1.0
135	1.0

To examine the contours of constant amplitude over a 1×1 km area, 150 patterns were formed at 10 second intervals as described in Section 5.5. The design parameters were the same as 7.9 except the velocity V was set at 52.5m/s, for which the true velocity of the surface should be about 100m/s. As mentioned above the axial ratio will be 1.1. From the 150 ellipses derived, the axial ratio varied from 1.02 to 2.49, with a median value of 1.38 and a 95 percentile of 2.07. Examples of the contours of constant amplitude over the 1×1 km area are shown in Figures 7.1 and 7.2. These contours were derived 10 seconds apart in time.

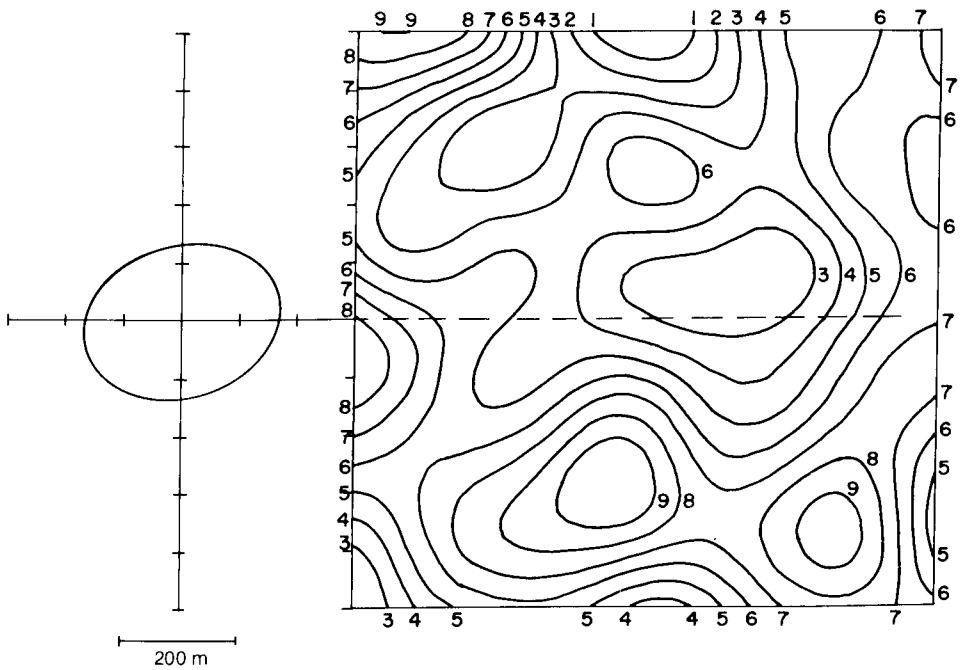

Figure 7.2 Contours of constant amplitude over a 1 × 1 km area for Model 3. The design parameters are defined in 7.9. The correlation ellipse has an axial ratio of 1.26.

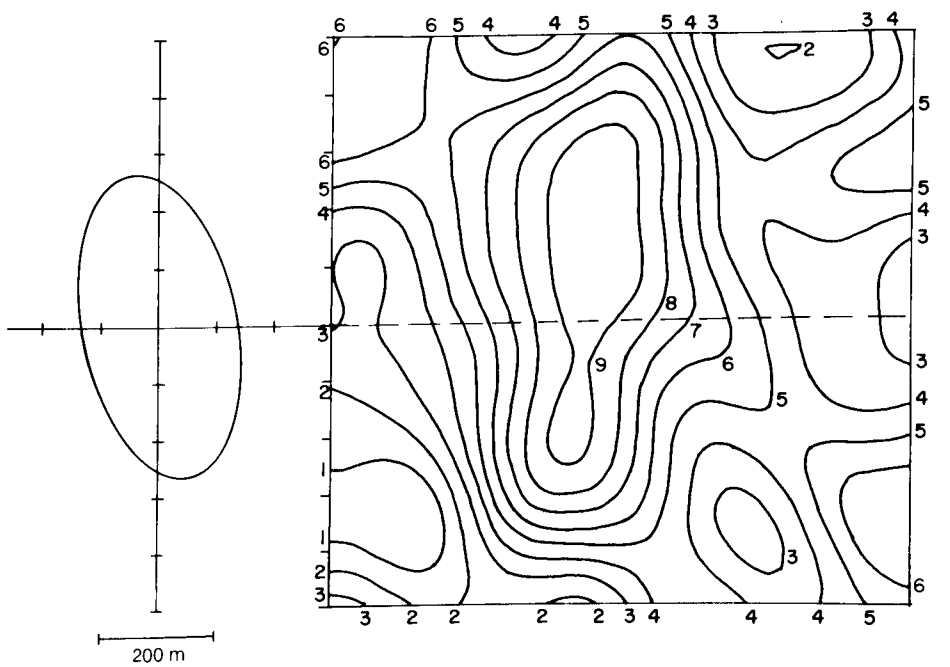

Figure 7.3 As for Figure 7.2, except that it is 10 seconds later. The correlation ellipse axial ratio is 1.86.

8. MODEL 4

8.1 THE CORRELATION FUNCTION

From Section 4 the correlation function for this model is

$$\rho_{r,\theta,\tau} = \frac{\left\langle \sum_{k=0}^{\infty} \sum_{\delta\phi=-\infty}^{\infty} \sum_{\delta V=-\infty}^{\infty} A_k^2 \cos(k(r\cos(\phi+\delta\phi+\theta)-(V+\delta V)\tau)) \right\rangle}{\left\langle \sum_{k=0}^{\infty} A_k^2 \right\rangle}. \tag{8.1}$$

The solution for 8.1 is given by Integral 4 in the Appendix, i.e.,

$$\rho_{r,\theta,\tau} = D + E,$$

where

$$\begin{aligned}
D &= \sum_{n=0}^{\infty} q \cos\frac{n\pi}{2} e^{-\frac{n^2\mathrm{Var}(\phi)}{2}} \cos n(\phi+\theta)\, C_m, \\
E &= \sum_{n=0}^{\infty} \sin\frac{n\pi}{2} e^{-\frac{n^2\mathrm{Var}(\phi)}{2}} \cos n(\phi+\theta)\, S_m, \\
C_m &= \sum_{m=0}^{\infty} \cos\frac{m\pi}{2} \frac{r^{n+2m}}{2^{n+2m} m!(n+m)!} \sum_{p=0}^{\infty} \cos\frac{p\pi}{2} \frac{(V\tau)^p}{p!} \frac{s\,1^{\frac{n+2m+p}{2}:2}}{(s^2+\tau^2\mathrm{Var}(V))^{\frac{1+n+2m+p}{2}}}, \\
S_m &= \sum_{m=0}^{\infty} \cos\frac{m\pi}{2} \frac{r^{n+2m}}{2^{n+2m} m!(n+m)!} \sum_{p=0}^{\infty} \sin\frac{p\pi}{2} \frac{(V\tau)^p}{p!} \frac{s\,1^{\frac{n+2m+p}{2}:2}}{(s^2+\tau^2\mathrm{Var}(V))^{\frac{1+n+2m+p}{2}}}
\end{aligned} \tag{8.2}$$

and $q = 1$ for $n = 0$; else $q = 2$.

This model differs from the previous model only in the way the random temporal changes are introduced. In Model 3 they were introduced by way of $\mathrm{Var}(\omega)$, in this model they are introduced by way of $\mathrm{Var}(V)$. Thus, what was said for Model 3 concerning the true velocity of the surface derived for $\mathrm{Var}(\omega) = 0$, is also true for Model 4 with $\mathrm{Var}(V) = 0$. The same is also true for the ratio of σ_x to σ_a. Where this model differs from Model 3 is the way this ratio varies with $\mathrm{Var}(V)$ compared with $\mathrm{Var}(\omega)$ of the latter model. This variation is shown in Table 8.1. Values of V_a and V_d, expressed as a percentage of V_t at r=100m, are also included in the Table. The variance of δV is expressed as a fraction of V.

If the values in Table 8.1 are compared with their corresponding values in Table 7.2, it will be noted that there is little difference between V_d and σ_x/σ_a derived for either model for random temporal changes.

TABLE 8.1

Variation of correlation parameters as a function of $\mathrm{Var}(V)$ *and r for* $\mathrm{Var}(\phi) = 65^0$ *and* $\sigma = 2s$.

	$r = 100m$				$r = 200m$			
$\mathrm{Var}(V)^{1/2}$	$\%V_a$	$\%V_d$	σ_x^-/σ_a	σ_x^+/σ_a	$\%V_a$	$\%V_d$	σ_x^-/σ_a	σ_x^+/σ_a
$0.0V$	100	56	1.04	1.03	91	64	1.14	1.08
$0.5V$	124	55	1.00	1.07	114	58	1.07	1.19
$1.0V$	198	54	1.00	1.08	176	55	1.07	1.21

8.2 FILTERING

Following the usual procedure, 25 sets of time-series were derived from the design parameters given below,

$$\begin{aligned} \mathrm{Var}(\phi)^{1/2} &= 65^0, & \mathrm{Var(V)}^{1/2} &= .75V, \\ V &= 100m/s, & \sigma &= 2.12s. \end{aligned} \tag{8.3}$$

From these parameters the expected value of $V_t = 183.0m/s$, $\sigma_a = 2.0s$ and the axial ratio, as for Model 3, is 1.1. The mean values of various correlation parameters, before and after filtering, are shown in Table 8.1. A value of n=2 was used because, for this value, the mean value of σ_a was reduced from 2.02s to 1.18s. This result is analogous to that for Model 2. The values of V_a and V_d are expressed as a percentage of V_t.

TABLE 8.2

Comparison of V_a *and* V_d *before and after the use of a high-pass filter. The design parameters are as in 8.3.*

Filter	$\%V_a$	$\%V_d$	ρ_m
nil	160	54	.957
$1-10$	163	63	.941
$1-20$	179	66	.928
$n=2$	168	67	.928

A comparison of the values in Table 8.2 with those in Table 7.3 (Model 3) shows that there is little difference between the two approaches for introducing the random temporal changes into the models.

8.3 SIMILAR FADES ANALYSIS

The data used in the previous section were also subjected to SFA and the results are presented in Table 8.3. As there was good agreement with V_t over the range of ρ_m's used, only section lengths of $2\sqrt{(\pi)}\sigma_a$ were used.

8.4 CORRELATION ELLIPSE

The variation of V_f as function of r is shown in Table 8.4. The design parameters are as for Table 8.1.

TABLE 8.3

Values of V_1 and V_2 from SFA as a function of ρ_m. The values are expressed as a percentage of V_t at r=100m. The design parameters are as in 8.3.

ρ_m	*%sections*	$\%V_1$	$\%V_2$
.75	75	179	103
.80	70	177	104
.85	65	173	109
.90	55	168	110
.95	35	164	123

TABLE 8.4

V_f as a function of r for various values of Var(V) *.The values are expressed as a percentage of V_t at r=100m. The design parameters are as those used for Table 8.1.*

$Var(V)^{1/2}$	$r = 100m$	$r = 100m$
$0.0V$	75	76
$0.5V$	83	81
$1.0V$	104	98

It will be noted from this Table that the changes, if anything, are small and negative.

Because Models 3 and 4 are identical with respect to random spatial changes, the information given in the previous section for Model 3 concerning the axial ratio of the correlation ellipse as a function of Var(ϕ) applies equally to Model 4.

With respect to the amplitude contours over a 1×1 km area, the contours were computed with the parameters of 8.3 except that the velocity V=52.5 m/s. From the 150 ellipses derived, the axial ratio varied from 1.02 to 2.72 with a median value of 1.37 and a 95 percentile value of 2.11. These results are very similar to those for Model 3. An example of the amplitude contours is shown in Figures 8.1 and 8.2 for 2 patterns 10 seconds apart.

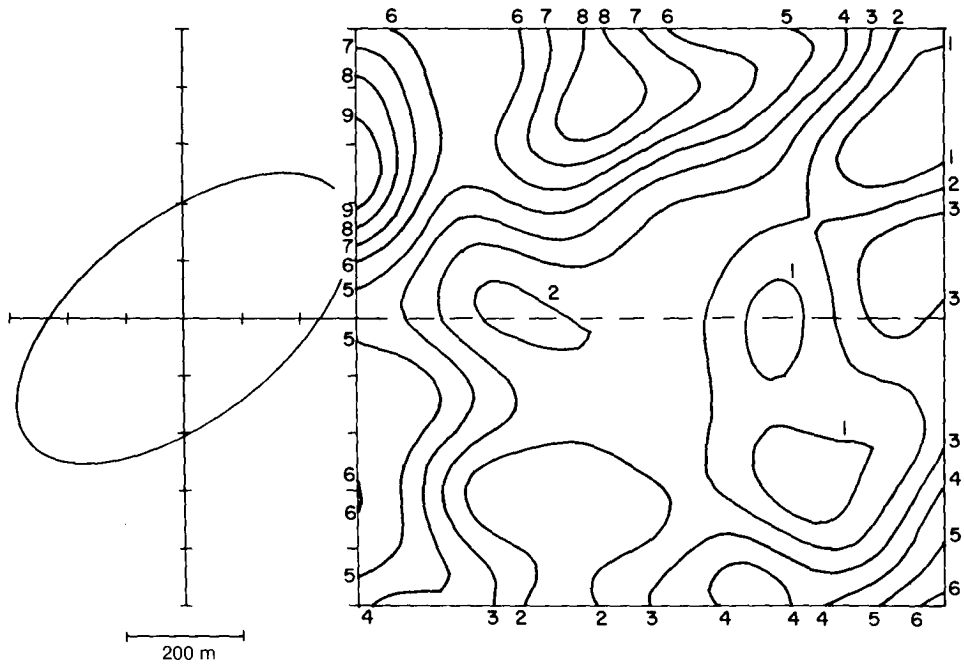

Figure 8.1 *Contours of constant amplitude over a 1 × 1 km area for Model 3. The design parameters are defined in 8.3. The correlation ellipse has an axial ratio of 2.01.*

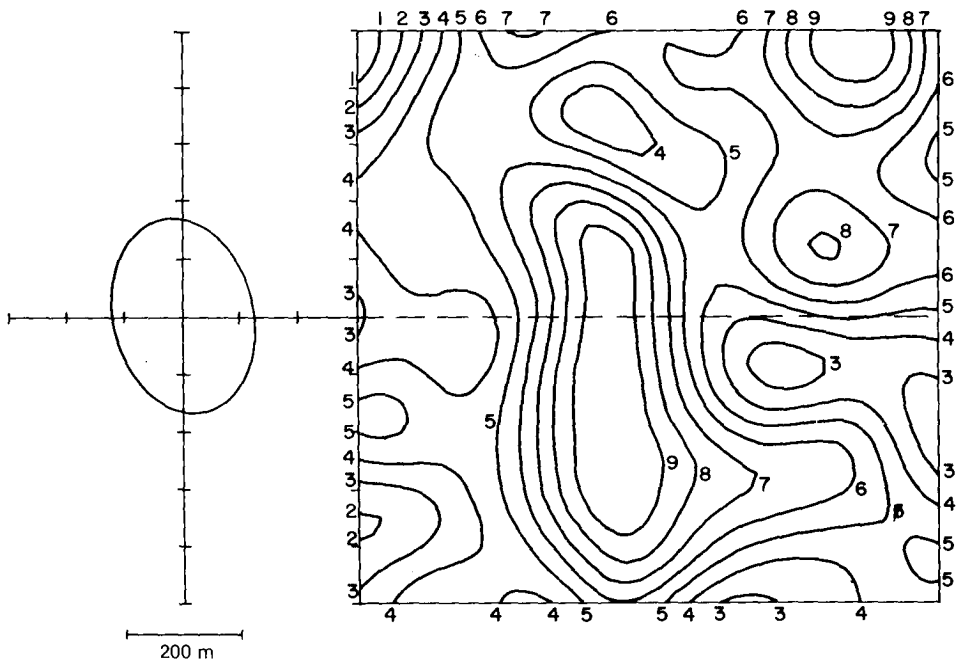

Figure 8.2 *As for Figure 8.1, except that it is 10 seconds later. The correlation ellipse axial ratio is 1.37.*

9. MODEL 5

In deriving the correlation function for this Model it is considered that the discussion can be considerably simplified by initially working in one dimensional space with only random spatial changes. For these conditions from 4.15 and 4.16

$$\rho_{r,\tau} = \frac{\langle A_\omega \cos\delta\alpha\, A_\omega \cos(\delta\alpha + r\,\delta\gamma)\cos(\omega(\tau - rH))\rangle}{[\langle A_\omega^2 \cos^2\delta\alpha\rangle\langle A_\omega^2 \cos^2(\delta\alpha + r\,\delta\gamma)\rangle]^{1/2}}. \tag{9.1}$$

As the random variables are independent of ω, and hence A_ω, consider the cosine term in the denominator, viz.,

$$\cos^2(\delta\alpha + r\delta\gamma) = 0.5(1 + \cos 2(\delta\alpha + r\,\delta\gamma)).$$

From the integrals of 7.6 it follows that

$$\langle 0.5(1 + \cos 2(\delta\alpha + r\,\delta\gamma))\rangle = 0.5(1 + e^{-2(\mathrm{Var}(\alpha)+r^2\mathrm{Var}(\gamma))}). \tag{9.2}$$

For this expression, if $\mathrm{Var}(\alpha) = 0$ then the mean varies asymtotically from 1 to 0.5 as r varies from 0 to ∞. To prevent this it is necessary to swamp the change in $r^2\mathrm{Var}(\gamma)$. A value of $\mathrm{Var}(\alpha) = 4$ is suggested for which

$$e^{-2\times 4} = 0.0003.$$

For this condition both the normalization terms in the denominator of 9.1, with respect to $\delta\alpha$ and $\delta\gamma$, will be very close to 0.5.

For the random variables in the numerator

$$\cos\delta\alpha\cos(\delta\alpha + r\,\delta\gamma) = \cos^2\delta\alpha\cos r\,\delta\gamma - cos\delta\alpha\sin\delta\alpha\sin r\,\delta\beta.$$

Since the mean of the sine terms are zero,then

$$\begin{aligned}\langle\cos^2\delta\alpha\cos r\,\delta\gamma\rangle &= 0.5(1 + e^{-2\mathrm{Var}(\alpha)})e^{-r^2\mathrm{Var}(\gamma)/2},\\ &= 0.5e^{-r^2\mathrm{Var}(\gamma)/2}.\end{aligned} \tag{9.3}$$

It follows from Model 1 that the correlation function of 9.1 is

$$\rho_{r,\tau} = e^{-\frac{r^2\mathrm{Var}(\gamma)}{2}} e^{-\frac{(\tau - rH)^2}{2\sigma^2}}. \tag{9.4}$$

Similar arguments can be presented with respect to random temporal changes, although the process is not as simple as for spatial changes. This arises because the correlation function is derived as a function of time for a given r. For this case, the amplitude term of the correlation function would be written as

$$\frac{\langle\cos(\delta\alpha + t\,\delta\beta)\cos(\delta\alpha + \delta\beta(t + \tau))\rangle}{\langle\cos^2(\delta\alpha + t\,\delta\beta)\rangle}.$$

For the denominator, at a given time t

$$\langle\cos^2(\delta\alpha + t\,\delta\beta)\rangle = 0.5(1 + e^{-2\mathrm{Var}(\alpha)+t^2\mathrm{Var}(\beta)}).$$

This mean must then be summed over all times t from t=0 to ∞. However, the end result is the same if $\mathrm{Var}(\alpha) > 4$ and the resultant correlation function

$$\rho(0,\tau) = e^{-\frac{\tau^2 \mathrm{Var}(\beta)}{2}} e^{-\frac{\tau^2}{2\sigma^2}}. \tag{9.5}$$

For the two dimensional case with both temporal and spatial random changes, the resultant correlation function has the same form as Model 1. Hence, the properties of Model 5 are the same as those described in Section 5 for Model 1.

The similarity with that of Model 1 can be seen in another way by expressing the correlation function as

$$\rho_{r,\tau} = \left\langle A_\omega^2 \cos r\,\delta\gamma \cos(\omega(\tau - rH)) \right\rangle. \tag{9.6}$$

For simplicity, it is assumed that $\mathrm{Var}(\alpha) = 0$ and that the normalization terms are unity. The above expression can be written as

$$\rho(r,\tau) = \left\langle \frac{A_\omega^2}{2} \cos(\omega(\tau - rH) + r\,\delta\gamma) \right\rangle + \left\langle \frac{A_\omega^2}{2} \cos(\omega(\tau - rH) - r\delta\gamma) \right\rangle. \tag{9.7}$$

As $\delta\gamma$ is normally distributed about zero, the two terms of the above expression have the same value, which is of the same form as Model 1.

Because of the similarity between Models 1 and 5, all discussion of the properties of Model 1 can be taken as also applying to Model 5.

10. SUMMARY

10.1 INTRODUCTION

For comparison purposes some of the more important properties of the various models are listed below. It will be remembered that the correlation function of Model 5 is of the same form as Model 1, so that any information on Model 1 applies equally to Model 5. The true velocities for Models 1 and 2 are 100m/s. The velocities for Models 3 and 4 are expressed as a percentage of V_t.

10.2 FILTERING

The values of V_d obtained from the data for each of the models, before and after filtering, are given in Table 10.2.1. The high-pass filtering was obtained by deleting the first 20 harmonics from the data. The changes in ρ_m are presented in Table 10.2.2.

TABLE 10.2.1

Values of V_d from FCA before and after filtering.

Model	*Before*	*After*	*%Change*
1	49	96	96
2	56	86	54
3	51	64	25
4	54	66	22

TABLE 10.2.2

ρ_m before and after filtering. The design value of ρ_m is also included in the Table.

Model	*Design*	*Before*	*After*
1	.91	.91	.91
2	.88	.88	.82
3	.97	.97	.95
4	.96	.96	.93

10.3 SIMILAR FADES ANALYSIS

The values of V_2 from SFA for each of the models, for various levels of ρ, are given in Table 10.3.

It has been shown that the values for Model 3 can be increased to close to the true velocity by using section lengths of $4\sqrt{(\pi)}\sigma_a$.

TABLE 10.3

Values of V_2 from SFA for various levels of ρ_m. Section lengths $2\sqrt{(\pi)}\sigma_a$.

Model	$\rho_m =$	.75	.80	.85	.90
1		101	102	103	106
2		106	111	116	124
3		77	77	78	83
4		103	104	109	110

10.4 THE LOW-VELOCITY EFFECT AND WEIGHTING METHOD

The values of V_d obtained from FCA and the weighting method are compared in Table 10.4.

TABLE 10.4

V_d from FCA and weighting method.

Model	*FCA*	*Weight*
1	50	49
2	56	40
3	51	49
4	54	43

It will be noted that for Models 2 and 4, the values from the weighting method are low compared with FCA. This could be due to the fact that σ_x/σ_a is greater than 1 and tends to give a higher value than expected for FCA. While this explanation appears valid for Model 2, it is questionable with respect to Model 4, as shown by the values of σ_x/σ_a given in Table 10.4.

10.5 THE RATIO OF σ_x TO σ_a

The ratios of σ_x to σ_a as a function of r are given in Table 10.5. The values are for the case where the random temporal changes are zero. It will noted that the effect is more pronounced with Model 2.

TABLE 10.5

Ratios of σ_x to σ_a as function of r

	$r = 100m$		$r = 200m$	
Model	σ_x^-/σ_a	σ_x^+/σ_a	σ_x^-/σ_a	σ_x^+/σ_a
2	1.12	1.12	1.41	1.41
3/4	1.04	1.03	1.14	1.08

10.6 V_d AS A FUNCTION OF r

The variation of V_d as a function of r is given in Table 10.6. These values are for the condition of no random temporal changes. Again Model 2 is affected more than Models 3 and 4.

TABLE 10.6

V_d as a function of aerial spacing.

Model	$r = 100m$	$r = 200m$	*%Change*
2	59	83	41
3/4	56	64	14

10.7 CORRELATION ELLIPSE

Variation of V_f as a function of r is shown in Table 10.7.1 for the case where random temporal changes are zero. It will be noted from this Table that the greatest change is for Model 2.

Table 10.7.1

V_f as a function of r.

Model	$r = 100m$	$r = 200m$
2	77	91
3/4	75	76

The distribution of the axial ratios from the 150 correlation ellipses for each model are summarized in Table 10.7.2.

TABLE 10.7.2

The range of axial ratios and their 50 and 95 percentile levels.

Model	*Range*	50%	95%
1	1.00 – 2.66	1.46	2.19
2	1.04 – 2.52	1.40	2.07
3	1.02 – 2.49	1.38	2.07
4	1.02 – 2.72	1.37	2.11

As can be seen from Table 10.7.2, the ellipse properties of the various models are very similar.

11. DISCUSSION

11.1 FULL CORRELATION ANALYSIS

Of the 5 models of moving random surfaces discussed in this report, only Models 1 and 5 satisfy the necessary conditions for the full correlation method of Briggs et.al. For these two models it is shown theoretically that the two correlation velocities, apparent velocity

$$V_a = (1 + \sigma^2 \mathrm{Var}(\omega))\mathrm{V}_t, \tag{11.1}$$

and the drift velocity

$$V_d = V_t/(1 + \sigma^2 V_t^2 \mathrm{Var}(k_\phi)), \tag{11.2}$$

where V_t is the true velocity of the surface in the direction ϕ, $\mathrm{Var}(\omega)$ is a measure of the random temporal changes and $\mathrm{Var}(\mathrm{k}_\phi)$ the spatial changes in the direction of motion ϕ.

From 5.2, it follows that the spatial auto-correlation functions in the direction of motion and at right angles to this direction are

$$\rho_{r,\phi,0} = e^{-r^2(1 + s^2 \mathrm{Var}(k_\phi))/2s^2} \tag{11.3}$$

and

$$\rho_{r,(\phi+\pi/2),0} = e^{-r^2 \mathrm{Var}(k_{(\phi+\pi/2)})/2s^2}, \tag{11.4}$$

where $s = V_t\sigma$.

It follows from 11.2 that, if there are random spatial changes in the direction of motion, then the correlation velocity V_d will be less than V_t. While random surfaces for Models 1 and 5 can be designed with $\mathrm{Var}(\omega) \neq 0$ and $\mathrm{Var}(k_\phi) = 0$, it follows from 11.4 that, if the correlation ellipse is to have a finite axial ratio, then there must be random spatial changes at right angles to the direction of motion. It is considered that such surfaces, while possible, are unrealistic and impracticable.

Models 2, 3 and 4 fail to satisfy the conditions for FCA, basically because $\sigma_x \neq \sigma_a$. However, if the correlation functions of these models are subjected to FCA, then, as shown in this report, interesting results are found.

11.2 SIMILAR FADES ANALYSIS

It has been shown that, even when a simple approach to SFA is applied to time-series from the 5 models, the velocities obtained are in much better agreement with V_t than those obtained from FCA. This is especially true for Models 1 and 4, as shown in Table 10.3.

It is considered that, if the improvements mentioned in Section 3 are applied, then even the velocities for Models 2 and 3 will be improved. It is also hoped that, because of the encouraging results reported

here, further work will place this method on a more rigorous base. In this respect it is considered that the work of Longuet-Higgins might be of some value.

11.3 IONOSPHERIC DRIFTS

Experimental evidence did not support the random screen model of Booker et.al. and it is now considered by most, if not all, workers in the field that the ground interference pattern is formed from the interference of a few radio waves specularly reflected from the ionosphere. For this reason one should be cautious in comparing the moving random surface models developed in this report with the radio interference patterns on the ground. However, as shown below, available experimental evidence suggest that the ground pattern has properties similar to Model 2.

11.3.1 σ_x/σ_a.

The early application of FCA was based on the straight-line method of Briggs et.al. However, as stated by Sales and Bowhill(1962), the 'Briggs straight line was frequently far from straight'. They assumed this defect to be due to sampling errors but, examination of a 'typical correlogram' presented in their Figure 2, shows

$$\sigma_a = 1.05m \quad \sigma_x^-/\sigma_a = 1.05, \quad \sigma_x^+/\sigma_a = 1.33.$$

For their work the radio frequency was 60khz, antenna spacing 3km and the reflection was from the D region of the ionosphere. For these conditions σ is in minutes rather than seconds.

Keneshea et.al.(1965), from E region data at 2.9 Mhz and r=104m, extended the work of Sales and Bowhill. From the typical correlogram in their Figure 5 it can be shown that

$$\sigma_a = 3s, \quad \sigma_x^-/\sigma_a = 1.33, \quad \sigma_x^+/\sigma_a = 1.33.$$

From the correlograms in Figure 4 of Chandra and Briggs

$$\sigma_a = 0.7s, \quad \sigma_x^-/\sigma_a = 1.45, \quad \sigma_x^+/\sigma_a = 1.23.$$

Their work was from D-region partial reflection data at 1.98Mhz with $r \approx 200m$.

Meek(1980), in discussing results obtained from D-region partial-reflection data, stated that 'it appears that the cross-correlograms are wider, on the average, than the auto correlograms'.

Shown in Figure 11.1 are the distributions of the ratios of σ_x/σ_a for 42 day-time E region records and 31 night-time F region records. These values were derived by the author from data recorded at Brisbane on 2.28Mhz with r=100m. σ_a and σ_x were derived from the least square fit of the correlation coefficients to a Gaussian curve. Thus, σ_x is the average of σ_x^- and σ_x^+.

All of the above experimental evidence suggests that the ground interference pattern behaves as predicted by Models 2, 3 and 4.

Golley and Rossiter(1970), from the use of a multi-aerial array at 1.98Mhz, found that V_d increased with increasing aerial spacing, whereas V_a showed no variation with r. They also found that the correlation ellipse tended to be aligned along the hypotenuse when small right-angled triangles for the antennae were used.

Models 2, 3 and 4 predict that V_d will increase with r, but only Model 2 predicts that V_a is independent of r. Moreover, Model 2 shows that V_f increases with r and hence the correlation ellipse will tend to be aligned along the direction of the antenna pair with the largest spacing.

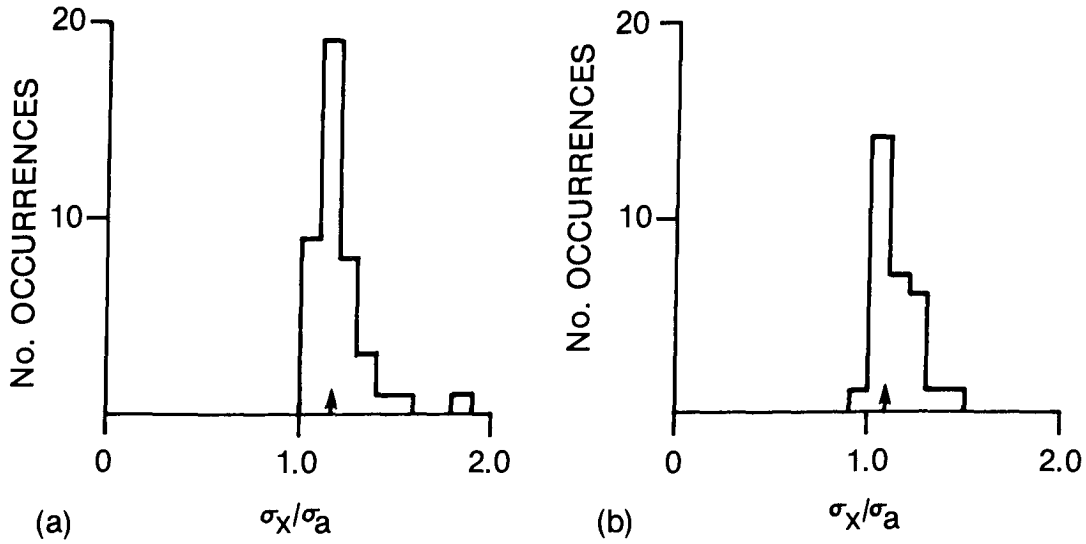

Figure 11.1: *Ratios of σ_x/σ_a for Brisbane data at 2.28 MHz.*
a) Daytime E-region.
b) Night-time F-region.

11.3.2 LOW V_d

Wright and Fedor(1967), from a simultaneous comparison of ionospheric winds obtained by FCA of ionospheric drift data and by luminous trail releases from rockets, found the luminous trail speed to be a factor of 2 greater than the speeds from FCA.

Sprenger and Schminder(1969), from a comparison of correlation speed with those obtained from meteor trails, found the former to be too low by a factor of 2 or more.

The author found the correlation speeds derived from E- and F-region records at Brisbane were too low by a factor of 2 or more compared with ionospheric speed derived by other methods at Brisbane.

All of the above results are consistent with the predictions of all of the models when random spatial changes are present in the direction of motion.

11.3.3 FILTERING

Sprenger and Schminder reported that after filtering their fading data with a high-pass filter, the correlation speed increased by a factor of 2 or more and were in much better agreement with the meteor trail speeds. They also reported that V_a was relatively unchanged after filtering.

The author also found similar results after filtering some F region records with a high-pass filter. V_d increased and V_a remained unchanged.

Chandra and Briggs also found experimentally that V_d increased after the use of a high-pass filter, but they argued that the effect on correlation speeds was no criterion that the speeds were too low. The same conclusion was arrived at for Model 1 from other reasoning and shown to be true both for Models 1 and 2 when there were no random spatial changes in the direction of motion. However, while ρ_m of Model 1 remains unaffected by filtering whether random spatial changes are present or not, ρ_m for Model 2 only remains unaffected if there are no random spatial changes. If these changes are present, then

ρ_m decreases after high-pass filtering and, conversely, increases after low-pass. From their experimental data, Chandra and Briggs found ρ_m to increase after low-pass filtering which strongly suggests that random spatial changes were present in their data and thus accounted for the increase in V_d.

Because random spatial changes must always be present in Models 3 and 4, the effect of filtering when no such changes are present cannot be considered for these models.

While all models predict that V_d will increase after high-pass filtering and that V_a will remain relatively unaffected, only Models 2, 3 and 4 predict that ρ_m will decrease after such filtering.

11.3.4 CHOICE OF MODEL

The above experimental evidence, taken *in toto*, strongly suggests that the radio interference pattern formed at the ground from a few rays specularly reflected from the ionosphere is of a form similar to Model 2 of this report. While much of the evidence also supports Model 3 and 4, the observation of Golley and Rossiter that the correlation ellipse tend to line up with its major axis in the direction of the antenna pair with the greatest spacing is peculiar to Model 2.

Also, there is much experimental evidence that the correlation ellipse can be oriented with neither axis in the direction of motion. If these results are real and not due to sampling errors, then the results automatically exclude Models 3 and 4.

Finally, the way random spatial changes are introduced into Models 3 and 4 is rather forced and restrictive, whereas, for Model 2, the approach is much freer and therefore more likely to occur.

11.4 RECOMMENDATIONS

From the work presented here, it is recommended that the use of the full correlation method of Briggs et.al. for ionospheric drifts analysis be treated with caution and that the Similar Fades Method (Variant 2) be used in its place. With regard to this latter method, it is hoped that further work will be done to refine it and place it on more rigorous grounds.

Acknowledgements: I am indebted to Dr. B. A. Senior who gave me hope and, thus, started me on the course of this work. I am also indebted to Dr C. E. Meek for his critical review of this work.

APPENDIX. INTEGRAL SOLUTIONS

A1 INTEGRAL 1

The integral to be considered in this section is

$$\frac{\int_{\omega=0}^{\infty} e^{-\frac{\omega^2\sigma^2}{2}} \int_{k=-\infty}^{\infty} e^{-\frac{k^2}{2\mathrm{Var}(k)}} \cos(\omega\tau - rk)dk\, d\omega}{\int_{\omega=0}^{\infty} e^{-\frac{\omega^2\sigma^2}{2}} dw \int_{k=-\infty}^{\infty} e^{-\frac{k^2}{2\mathrm{Var}(k)}} dk}, \qquad (A1.1)$$

where ω and k are independent variables.

In solving this integral only those sections pertinent to the discussion will be considered and it is assumed that, in the integration of the numerator with respect to a particular variable, its counterpart in the denominator is also included.

Expanding the cosine term of A1.1,then

$$\cos(\omega\tau - rk) = \cos\omega\tau\, \cos kr + \sin\omega\tau\, \sin kr.$$

Because $\sin kr$ is an odd function, its integration with respect to k will be zero. Using the integrals of 7.6, the integration of $\cos kr$ is

$$e^{-\frac{r^2\mathrm{Var}(k)}{2}}.$$

Similarly, the integration of $\cos\omega\tau$ with respect to τ is

$$e^{-\frac{\tau^2}{2\sigma^2}}.$$

Thus, the solution to integral A1.1 is

$$e^{\frac{-r^2\mathrm{Var}(k)}{2}} e^{-\frac{\tau^2}{2\sigma^2}}. \qquad (A1.2)$$

In the main body of the text τ may be a function of several variables, e.g., $\tau - rH$ and rk may be the sum of up to 3 random variables. In the latter case, not only their variances but also their covariances must be considered.

A2 INTEGRAL 2

The integral to be considered in this section is

$$\frac{\int_{\omega=0}^{\infty} e^{-\frac{\omega^2\sigma^2}{2}} \int_{H=-\infty}^{\infty} e^{-\frac{H^2}{2\mathrm{Var}(H)}} \cos(\omega\tau - \omega rH)dH\, d\omega}{\int_{\omega=0}^{\infty} e^{-\frac{\omega^2\sigma^2}{2}} dw \int_{H=-\infty}^{\infty} e^{-\frac{H^2}{2\mathrm{Var}(H)}} dH}, \qquad (A2.1)$$

where H and ω are independent variables.

As for Integral 1, expand the cosine term, neglect the sine term of the expansion and integrate with respect to H. The solution is

$$e^{-\omega^2 r^2 \mathrm{Var}(H)/2}.$$

This term modifies $e^{-\omega^2\sigma^2/2}$ to

$$e^{-\omega^2(\sigma^2+r^2\mathrm{Var}(H))/2}.$$

Then integrate with respect to ω and the solution of A2.1 is

$$\frac{1}{(1+r^2\mathrm{Var}(H)/\sigma^2)^{1/2}} e^{-\frac{r^2}{2\sigma^2(1+r^2\mathrm{Var}(H)/\sigma^2)}}. \qquad (A2.2)$$

For this integration, it should be noted that the coefficient of ω^2 in the numerator is $(\sigma^2 + r^2\mathrm{Var(H)})$, whereas in the denominator it is σ^2.

A3 INTEGRAL 3

The integral to be considered in this section is

$$\frac{\int_{k=0}^{\infty} e^{-\frac{k^2 s^2}{2}} \int_{\phi=-\infty}^{\infty} e^{-\frac{\phi^2}{2\mathrm{Var}(\phi)}} \int_{\omega=-\infty}^{\infty} e^{-\frac{\omega^2}{2\mathrm{Var}(\omega)}} \cos(k(r\cos(\Phi+\phi)-V\tau)+\omega\tau) d\omega\, d\phi\, dk}{\int_{k=0}^{\infty} e^{-\frac{k^2 s^2}{2}} dk \int_{\phi=-\infty}^{\infty} e^{-\frac{\phi^2}{2\mathrm{Var}(\phi)}} d\phi \int_{\omega=-\infty}^{\infty} e^{-\frac{\omega^2}{2\mathrm{Var}(\omega)}} d\omega}, \qquad (A3.1)$$

where ω, and k are independent variables.

Following the procedures from Integral 1 by expanding the outer cosine term of A3.1, integrating with respect to ω and rejecting the sine term, then the integral for the ω term is

$$e^{-\frac{r^2\mathrm{Var}(\omega)}{2}}. \qquad (A3.2)$$

Further expansion of the cosine term results in

$$\cos(kr\cos(\Phi+\phi))\cos kV\tau + \sin(kr\cos(\Phi+\phi))\sin kV\tau.$$

To integrate this with respect to ϕ it is necessary to expand the cos(cos) and sin(cos) terms into their power series of which a convenient form is

$$\cos(x\cos(y)) = J_0(x) - 2[(J_2(x)\cos 2y - J_4(x)\cos 4y + \cdots] \qquad (A3.3)$$

and

$$\sin(x\cos(y)) = 2[J_1(x)\cos y - J_3(x)\cos 3y + J_5(x)\cos 5y - \cdots], \qquad (A3.4)$$

where $J_n(x)$ is the Bessel function of the first kind and is

$$J_n(x) = \sum_{m=0}^{\infty} (-1)^m \frac{x^{n+2m}}{2^{(n+2m)}\, m!(n+m)!}. \qquad (A3.5)$$

For integration with respect to ϕ, the relevant portion of the n^{th} term is $\cos n(\Phi+\phi)$. On expansion of this cosine term and integration with respect to ϕ, it follows from the previous work that the solution is

$$\cos n\Phi e^{-\frac{n^2 \mathrm{Var}(\phi)}{2}}. \qquad (A3.6)$$

Finally, for integration with respect to k, it is necessary to expand $\cos(kV\tau)$ and $\sin(kV\tau)$ into their power series, which can best be represented as

$$\cos kV\tau = \sum_{p=0}^{\infty} \cos\frac{p\pi}{2}\frac{(kV\tau)^p}{p!}$$

and

$$\sin kV\tau = \sum_{p=0}^{\infty} \sin\frac{p\pi}{2}\frac{(kV\tau)^p}{p!}.$$

Considering the cos(cos) term first, then the relevant (n,m) term for k is combined with the p^{th} from $\cos(kV\tau)$ to produce

$$\frac{k^{n+2m}(kV\tau)^p}{p!}.$$

A solution for the integral associated with this term is given by Bierens de Haan(1939), Table 81.6, in the form

$$\int_{-\infty}^{\infty} e^{-\frac{x^2}{2p^2}} x^{2a}dx = 1^{a:2}p^{2a+1}\sqrt{(2\pi)},$$

where $1^{a:2}$ is in Kramps notation, viz,

$$c^{a:b} = c(c+b)(c+2b)(c+3b)\cdots(c+(a-1)b.$$

Applying this to A3.1 the integral with respect to k is

$$\frac{1^{\frac{(n+2m+p)}{2}:2}}{s^{2(n+2m+p)}}\frac{(V\tau)^p}{p!}. \qquad (A3.7)$$

Collecting the various values then the integral of A3.1 for the cos(cos) term is

$$e^{-\frac{r^2 \mathrm{Var}(\omega)}{2}}\sum_{n=0}^{\infty} q\cos\frac{n\pi}{2}e^{-\frac{n^2 \mathrm{Var}(\phi)}{2}}\cos n\Phi\, C_m,$$

where $q = 1$ for $n = 0$; else $q = 2$, and

$$C_m = \sum_{m=0}^{\infty}\cos\frac{m\pi}{2}\frac{r^{n+2m}}{m!(n+m)!}\sum_{p=0}^{\infty}\cos\frac{p\pi}{2}\frac{(V\tau)^p}{p!}\frac{1^{\frac{(n+2m+p)}{2}:2}}{s^{(n+2m+p)}}. \qquad (A3.8)$$

The integral for the sin(cos) term is very similar, viz.,

$$e^{-\frac{r^2 \mathrm{Var}(\omega)}{2}}\sum_{n=0}^{\infty}\sin\frac{n\pi}{2}e^{-\frac{n^2 \mathrm{Var}(\phi)}{2}}\cos n\Phi\, S_m,$$

where

$$S_m = \sum_{m=0}^{\infty}\cos\frac{m\pi}{2}\frac{r^{n+2m}}{m!(n+m)!}\sum_{p=0}^{\infty}\sin\frac{p\pi}{2}\frac{(V\tau)^p}{p!}\frac{1^{\frac{(n+2m+p)}{2}:2}}{s^{(n+2m+p)}}. \qquad (A3.9)$$

A4 INTEGRAL 4

The integral to be considered in this section is

$$\frac{\int_{k=0}^{\infty} e^{-\frac{k^2 s^2}{2}} \int_{\phi=-\infty}^{\infty} e^{-\frac{\phi^2}{2\mathrm{Var}(\phi)}} \int_{v=-\infty}^{\infty} e^{-\frac{v^2}{2\mathrm{Var}(v)}} \cos(k(r\cos(\Phi+\phi)-(V+v)\tau) dv\, d\phi\, dk}{\int_{k=0}^{\infty} e^{-\frac{k^2 s^2}{2}} dk \int_{\phi=-\infty}^{\infty} e^{-\frac{\phi^2}{2\mathrm{Var}(\phi)}} d\phi \int_{v=-\infty}^{\infty} e^{-\frac{v^2}{2\mathrm{Var}(v)}} dv}, \qquad (A4.1)$$

where k, ϕ and v are independent variables.

The solution for this integral follows along very similar lines to that for Integral 3 and much of what was said there will be taken for granted. Thus the integration with respect to ϕ will produce a term

$$\cos n\Phi e^{-\frac{n^2\mathrm{Var}(\phi)}{2}}. \qquad (A4.2)$$

In the first expansion of the outer cosine term of A4.1,the two terms with respect to v are

$$\cos k(V+v)\tau \text{ and } \sin k(V+v)\tau$$

The expansion and integration with respect to v of the cosine term will result in the term

$$\cos kV\tau\, e^{-\frac{k^2\tau^2\mathrm{Var}(v)}{2}},$$

and for the sine term

$$\sin kV\tau\, e^{-\frac{k^2\tau^2\mathrm{Var}(v)}{2}}.$$

Thus the relevant portions of the cos(cos) term for integration with respect to k are

$$e^{-\frac{k^2}{2}(s^2+\tau^2\mathrm{Var}(v))}\, k^{n+2m}(kV\tau)^p/p!.$$

The integration of this term produces

$$\frac{(V\tau)^p}{p!} \frac{1^{(n+2m+p):2}}{(s^2+\tau^2\mathrm{Var}(v))^{(n+2m+p)/2}} \frac{s}{\sqrt{(s^2+\tau^2\mathrm{Var}(v))}}.$$

Combining the relevant terms, the integral of the cos(cos) term is

$$\sum_{n=0}^{\infty} q\cos\frac{n\pi}{2} e^{-\frac{n^2\mathrm{Var}(\phi)}{2}} \cos n\Phi\, C_m,$$

where $q = 1$ for $n = 0$; else $q = 2$, and

$$C_m = \sum_{m=0}^{\infty} \cos\frac{m\pi}{2} \frac{r^{n+2m}}{m!(n+m)!} \sum_{p=0}^{\infty} \cos\frac{p\pi}{2} \frac{(V\tau)^p}{p!} \frac{1^{\frac{(n+2m+p)}{2}:2} s}{(s^2+\tau^2\mathrm{Var}(v))^{(1+n+2m+p)/2}}. \qquad (A4.3)$$

Similarly, it can be shown that the integral for the sin(cos) term is

$$\sum_{n=0}^{\infty} \sin\frac{n\pi}{2} e^{-\frac{n^2\mathrm{Var}(\phi)}{2}} \cos n\Phi\, S_m,$$

where

$$S_m = \sum_{m=0}^{\infty} \cos\frac{m\pi}{2} \frac{r^{n+2m}}{m!(n+m)!} \sum_{p=0}^{\infty} \sin\frac{p\pi}{2} \frac{(V\tau)^p}{p!} \frac{1^{\frac{(n+2m+p)}{2}:2} s}{(s^2+\tau^2\mathrm{Var}(v))^{(1+n+2m+p)/2}}. \qquad (A4.4)$$

REFERENCES

Awe, O., *J. Atmos. Terr. Phys.*, **26**: 1239-1255 (1964).

Bierens de Haan, D. *New Tables of Definite Integrals, G. E. Strechert and Co., New York.* (1939).

Booker, H. G., Ratcliffe, J. A. and Shinn, D. A. , *Phil. Trans.*, **A, 856** :579-609 (1950).

Bowman, G. G., *J. Atmos. Terr. Phys.*, **30** :721-734 (1968).

Briggs, B. H., *Radio Science,* **11** :817-819 (1976).

Briggs, B. H., Phillips, G. J. and Shinn, D. H., *Proc. Phys. Soc.,* **B63**:106-121 (1950).

Burke, M. J., *Radio Science,* **10** :1035-1036 (1975).

Burke, M. J. and Jenkinson, I. S., *Aust. J. Phys.*, **10** :378-386 (1957).

Chandra, H. and Briggs, B. H., *J. Atmos. Terr. Phys.*, **40** :541-548 (1978).

Felgate, D. G. and Golley, M. G., *J. Atmos. Terr. Phys.*, **33** :1353-1369 (1971).

Golley, M. G. and Rossiter, D. E., *J. Atmos. Terr. Phys.* , **32** :1215-1233 (1970).

Keneshea, T. J., Gardiner, M. E. and Pfister, W., *J. Atmos. Terr. Phys.* ,**27** :7-30 (1965).

Longuet-Higgins, M. S., *Phil. Trans. Roy. Soc.*, **249** :321-387 (1957).

Longuet-Higgins, M. S., *Phil. Trans. Roy. Soc.*, **250** :157-174 (1957).

Meek, C. E., *J. Atmos. Terr. Phys.*, **42** : 835-839 (1980).

Mitra, S N., *Proc. Inst. Elect. Engrs.*, **96** : Part III, 441-450 (1949).

Ratcliffe, J. A., *Reports on Prog. in Physics,* **19** :188-267 (1956).

Sales, G. S. and Bowhill, S. A., *J. Atmos. Terr. Phys.*, **24** :451-465 (1962).

Sprenger, K. and Schminder, R., *J. Atmos. Terr. Phys.*, **31**:1085-1098 (1969).

Thomas, J. A. and Burke, M. J., *Aust. J. Phys.*, **9**: 440-453 (1956).

Wright, J. W. and Fedor, L. S., *Space Research VII , North-Holland Publishing Co. , Amsterdam*: 67-72 (1967).

Wright, J. W. and Pitteway, M. L. V., *Radio Science,* **13**: 189-209 (1978).